AN ABSTRACT OF THE THESIS OF

RODNEY DEAN COOKE (Name) for the DOCTOR OF PHILOSOPHY (Degree)

in PHYSICAL CHEMISTRY (Major) presented on October 24, 1972 (Date)

Title: INFRARED, REFLECTION AND RAMAN SPECTRA OF SODIUM AND POTASSIUM BIFLUORIDE

Abstract approved: J. C. Decius

Single crystal infrared and Raman studies using samples of known orientation relative to the crystal axes are inherently capable of yielding more information than polycrystalline samples. Such information includes the assignment of modes for coupled vibrations in the unit cell, and the measurement of the transition strength in the infrared case, which is proportional to $(\frac{\partial \mu}{\partial q})_0^2$. Since it is difficult and often practically impossible to prepare sufficiently thin sections for infrared transmission experiments, infrared reflectivity is the preferred single crystal technique in most cases. Reflectivity can profitably be studied as a function of angle of incidence and in general different results are expected and found for T_E and T_M polarizations ($\vec{E}$ vector respectively perpendicular and parallel to the plane of incidence).

In order to test theories of the coupling of molecular vibrations

in crystals, the bending vibrations (ν_2's) of the acid fluoride ion (HF_2^-) in $NaHF_2$ and KHF_2 were studied in the infrared region by varying the amount of deuterium in the sample. The samples ranged from 2% to 96% DF_2^- in $NaHF_2$ and from 3% to 93% DF_2^- in KHF_2. The isotopically dilute (uncoupled) bending frequencies of DF_2^- as well as HF_2^- were obtained for both salts.

Polarized reflection spectra were recorded with incident angles of 10° and 37° for single crystalline KHF_2 and for well-oriented polycrystalline $NaHF_2$. These spectra were compared to theoretical reflection curves to aid in the assignments of the transverse and longitudinal frequencies associated with the bending vibrations ($\nu_2(E_u)$ of $NaHF_2$ and $\nu_2(A_{2u})$ and $\nu_2(E_u)$ for KHF_2). Also, quasi-longitudinal reflection bands (maximum reflectivity which occurs at a higher frequency than expected) were observed for both bending vibrations of KHF_2 with an angle of incidence of 37°. These quasi-longitudinal bands were helpful in determining the damping constants, the transverse and longitudinal frequencies at the bending vibrations of KHF_2.

In order to use the transverse-longitudinal frequency separation to calculate $(\frac{\partial \mu}{\partial q})_0$ (and also the shift of frequency of the pure crystal relative to the decoupled frequency) it is necessary to employ a measure of the effective field in a polarizable medium. Previous authors have either assumed the Lorentz field, which is appropriate only to

the cubic case, or have neglected the (high frequency) polarizability completely. In the present work this effective field was evaluated in terms of the individual ionic polarizabilities and lattice sums of the dipole-dipole coupling tensor. The polarizabilities were calculated from the optical refractive indices with the aid of the B matrix defined as $\underset{\approx}{B} = (\underset{\approx}{E}-\underset{\approx}{\alpha}\underset{\approx}{S})^{-1}$ where $\underset{\approx}{S}$ is the lattice sum of the dipole coupling tensor and α is the polarizability tensor and the B elements were subsequently used in the calculation of $(\frac{\partial \mu}{\partial q})_0$.

Using the transverse and longitudinal frequencies of the ν_2 modes, the uncoupled frequencies as well as the dipole moment derivatives of each of the bands were calculated by assuming that the only interaction in the crystal is a dipole-dipole interaction. The uncoupled frequencies (calculated) were compared to the experimental values of the isotopically dilute frequencies.

Although it is believed that the theory correctly relates the transverse-longitudinal frequency splitting to $(\frac{\partial \mu}{\partial q})_0$, the calculated uncoupled frequencies are not in good agreement with the isotopically dilute frequencies. This may be due to terms in the coupling Hamiltonian other than those arising from the molecular dipoles. If the forces involved are short range, such terms would affect the location of the uncoupled frequencies but would not influence the transverse-longitudinal splittings.

The Raman spectrum of single crystal KHF_2 showed peaks at

608.5 cm^{-1}, 600 cm^{-1}, 143 cm^{-1}, 139.5 cm^{-1} and 100.5 cm^{-1}, and these were assigned to $\nu_1(B_{2g})$, $\nu_1(A_g)$, R-(E_g), R-(B_{1g}) and T+(E_g), respectively. The two librational frequencies (143 cm^{-1} and 139.5 cm^{-1}) were not previously separated. Raman spectra of powdered $NaHF_2$ were obtained and agreed quite well with previous results.

Infrared, Reflection and Raman Spectra of Sodium and Potassium Bifluoride

by

Rodney Dean Cooke

A THESIS

submitted to

Oregon State University

in partial fulfillment of
the requirements for the
degree of

Doctor of Philosophy

June 1973

APPROVED:

Redacted for privacy

Professor of Chemistry

in charge of major

Redacted for privacy

Chairman of Department of Chemistry

Redacted for privacy

Dean of Graduate School

Date thesis is presented 24 October 1972

Typed by Clover Redfern for Rodney Dean Cooke

ACKNOWLEDGEMENTS

First I wish to express my gratitude to Dr. J.C. Decius for his assistance and inspiration in the last five years. Also I would like to thank Dr. R.E. Carlson and Dr. Roger Frech for many helpful discussions. My wife deserves particular credit for enabling me to concentrate on my work at Oregon State University.

Partial fianancial support of this research by the National Science Foundation is gratefully acknowledged.

TABLE OF CONTENTS

LIST OF TABLES

LIST OF FIGURES

INFRARED, REFLECTION AND RAMAN SPECTRA OF SODIUM AND POTASSIUM BIFLUORIDE

I. INTRODUCTION

The structure and the vibrational spectra of sodium and potassium acid fluoride have been studied previously by several techniques. These include calorimetry (1, 2), x-ray and neutron diffraction (3, 4, 5, 6), neutron inelastic scattering (7, 8), Raman (8, 9), infrared (8, 10, 11) and reflection spectroscopy (12, 13). These studies have established definitely that the bifluoride ion $(FHF)^-$ is linear and symmetric ($D_{\infty h}$) in both crystals.

This study was undertaken to investigate the role of dipolar coupling in the bending vibration in these crystals. The asymmetric stretching vibrations were not studied because of the very unusual characteristics of the modes. The isotopic dilution technique was used to determine the degree of coupling (14). This method has been used previously by Rush, Schroeder, and Melveger (8) (hereafter RSM). This study hoped to improve their frequencies for the isolated DF_2^- in HF_2^- and obtain a high enough deuterated species to observe the isolated bending vibration of HF_2^- in the DF_2^- lattice with each salt. The frequencies associated with the isotopically dilute bending vibration will be called the uncoupled frequencies, while the frequencies of the pure species will be called the coupled frequencies.

The uncoupled frequencies can be compared to calculated values

by applying the dipolar coupling method of Decius (15). Before this can be performed, the transverse (ν_{2T}) and the longitudinal (ν_{2L}) frequencies associated with these bending vibrations (ν_2) must be determined. Reflectivity measurements were undertaken to determine these frequencies. Reflection spectra at an oblique angle (37°), as well as near normal (10°), were taken of both crystals. Both of the reflectivity measurements at the two angles were compared to theoretical reflection curves to aid in the assignment of ν_T and ν_L.

Raman scattering experiments were performed on single crystals of KHF_2 in hopes of resolving the two librational fundamentals. In previous Raman studies only two of the three active lattice modes were observed (8, 9), and these were attributed to the translational motion of the potassium ion and accidentally degenerate librational modes. Also the Raman experiments were done on powdered sodium bifluoride to aid in the assignments of the librational frequencies of the potassium salt.

Crystal Structures

The crystal structures of $NaHF_2$ and $NaDF_2$ have been determined by x-ray and neutron diffraction studies, Table I-1 (3, 4). Since the lattice parameters of both salts are the same within their experimental error, they will be assumed to be identical. These studies have shown that $NaH(D)F_2$ belongs to the space group $D_{3d}^5(R\bar{3}M)$. The

Table I-1. Lattice parameters of KHF_2, $NaHF_2$ and $NaDF_2$.

	$NaHF_2$	$NaDF_2$
a = b =	3.476(2) Å	3.474(2) Å
c =	13.76(1) Å	13.75(1) Å
D(F-X-F) =	2.264(3) Å	2.265(7) Å

	KHF_2
a = b =	5.67 Å
c =	6.81 Å
D(F-X-F) =	2.277(6) Å

primitive unit cell is trigonal and contains only one molecule (Figure I-1), while the hexagonal (crystallographic) unit cell contains three molecules. The structural data for both the primitive and the non-primitive cell are summarized in Table I-1.

Neutron and x-ray diffraction have established that KHF_2 and KDF_2 crystallize into tetragonal unit cells which belong to the space group D_{4h}^{18}(I 4 mcm) (4, 5, 6). The primitive unit cell contains two molecules, while the crystallographic unit cell contains four molecules. The bifluoride and the potassium ions are situated in alternate horizontal planes with the axes of the bifluoride ion being perpendicular to one another. The layers of the bifluoride ions alternate in direction; therefore looking down the optic (Z) axis, the ions would appear to be mutually perpendicular, as shown in Figure I-2. The structural data for KHF_2 and KDF_2 are summarized in Table I-1.

Degrees of Freedom

There are four atoms comprising the smallest (primitive) cell for either $NaHF_2$ or $NaDF_2$, thus twelve degrees of freedom must fall within the six symmetry species of the space group, D_{3d}^5. The symmetry species were determined by the correlation technique or with the use of a correlation diagram (16). This diagram (Figure I-3) illustrates site and factor group slitting. In applying this method, care must be exercised in selecting the correct axis in the site

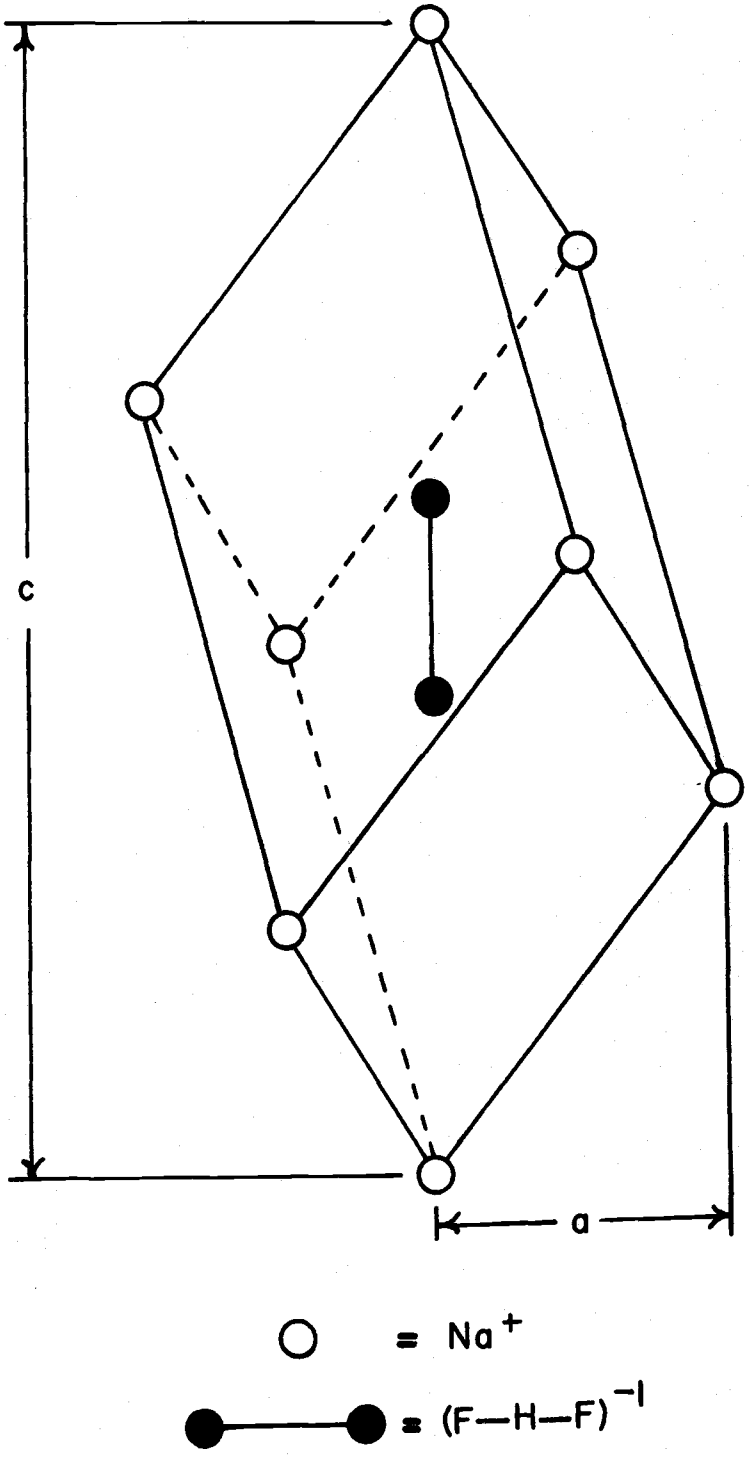

Figure I-1. General view of the crystal structure of $NaHF_2$.

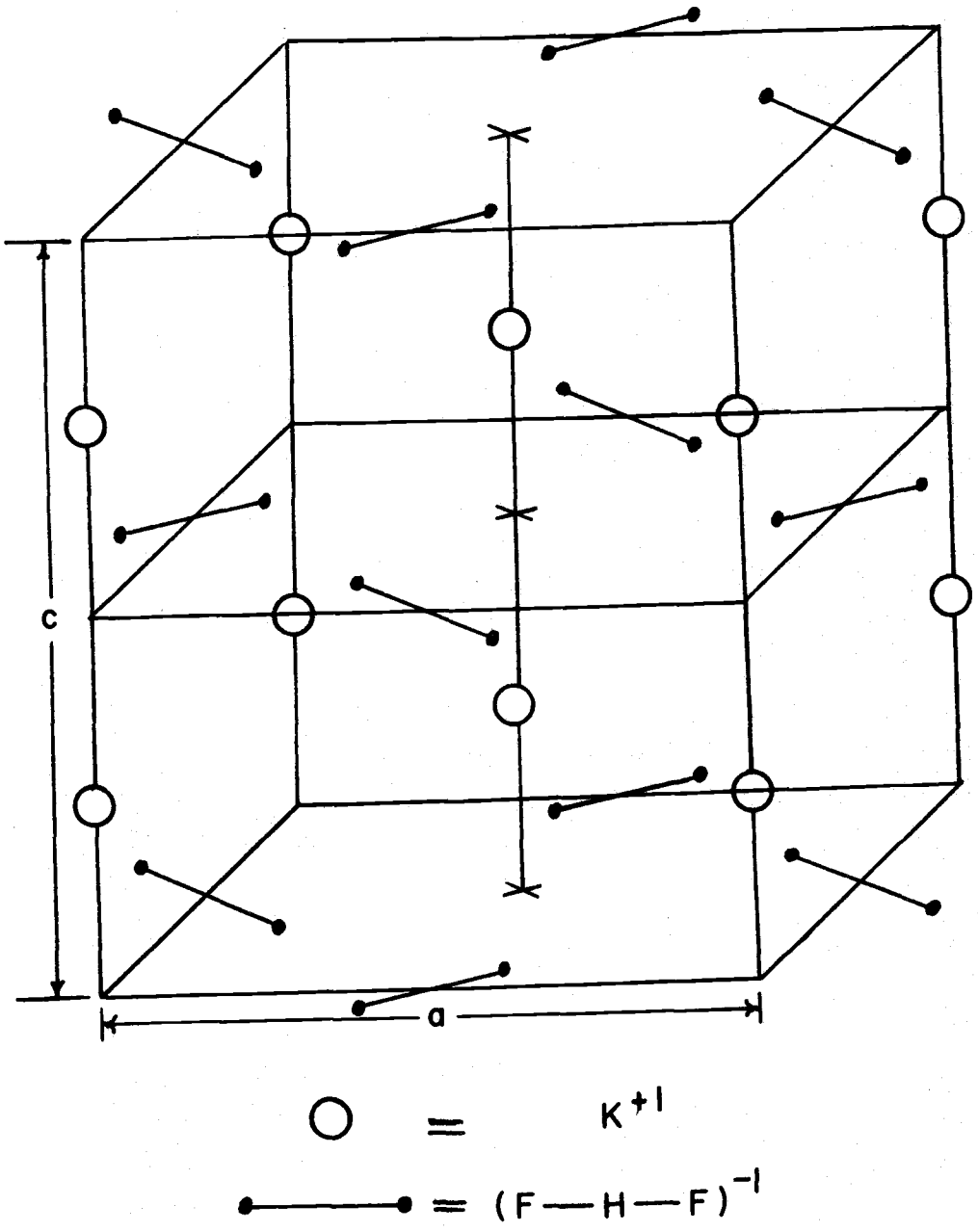

Figure I-2. General view of the crystal structure of KHF_2.

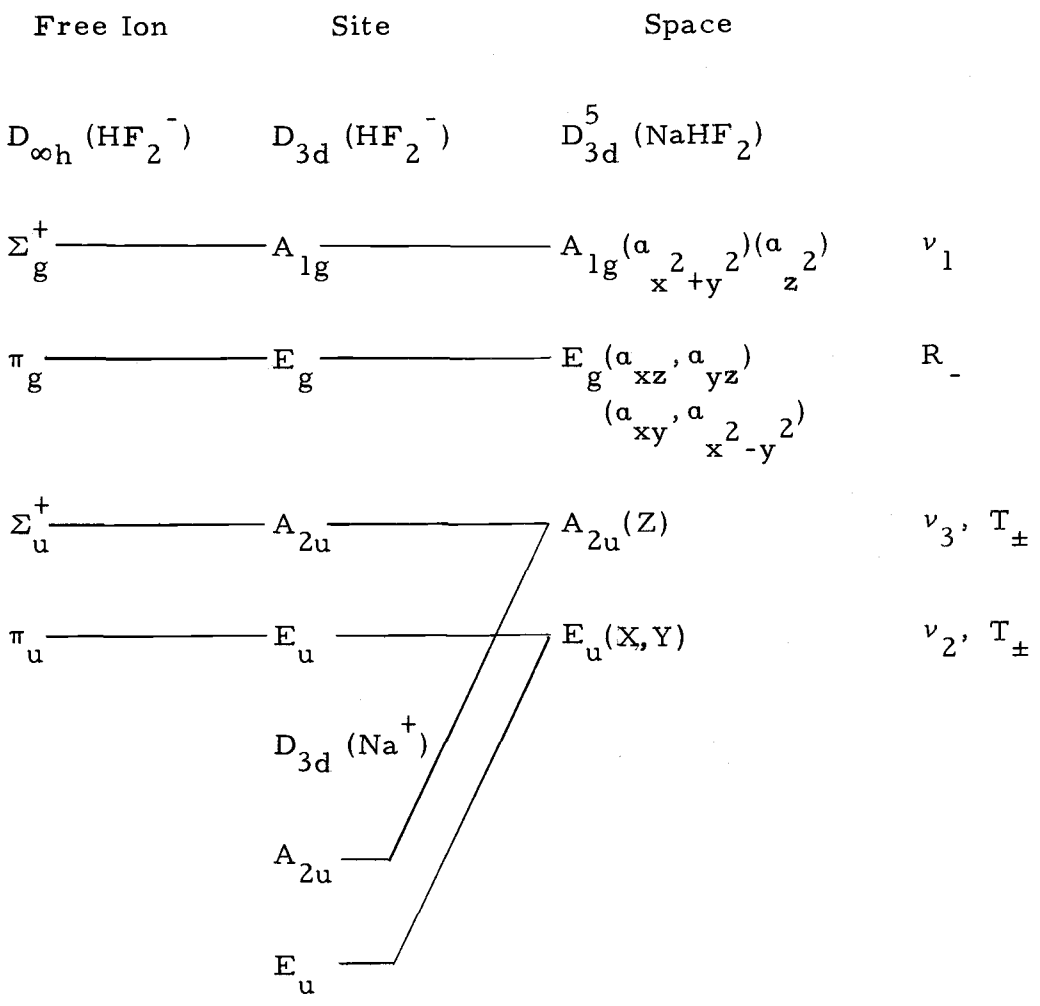

Figure I-3. Correlation diagram for $NaHF_2$.

symmetry as well as in subtracting out the three degrees of freedom associated with the acoustic modes. In the correlation diagram of $NaH(D)F_2$, the ν_i's represent internal vibrations and R_- and $T_\pm$ represent the librational modes of the anion (-) and the translational modes of both the anion (-) and the cation (+), respectively.

For $KH(D)F_2$, there are eight atoms that comprise the primitive cell, hence 24 degrees of freedom must fall within the ten symmetry species of the space group, D_{4h}^{18}. The correlation diagram for $KH(D)F_2$ is given in Figure I-4. This diagram illustrates doubling of modes ($B_{3g} = E_g$), site group splitting ($\pi_g = B_{1g}$ and B_{3g}), factor group splitting ($A_g = A_{1g}$ and B_{2g}) and the right selection of the primary axis of the D_{2h} site. The acoustic modes were subtracted from both crystal correlation diagrams.

Correlation diagrams are more useful in solid state spectroscopy than a straight group theoretical method, such as that of Bhagawantan and Venkataraynda (17). The reasons are: (1) It can be seen immediately if the translatory motion depends on the mass of the anion (-), cation (+) or both (±); (2) It shows what type of splitting is involved; and (3) it shows if there is a doubling of the modes caused from having more than one molecule per primitive cell. In general, site group splittings are larger than factor group splittings.

From the correlation diagrams, the activity of each of the vibrational modes can be determined easily. A vibrational mode is

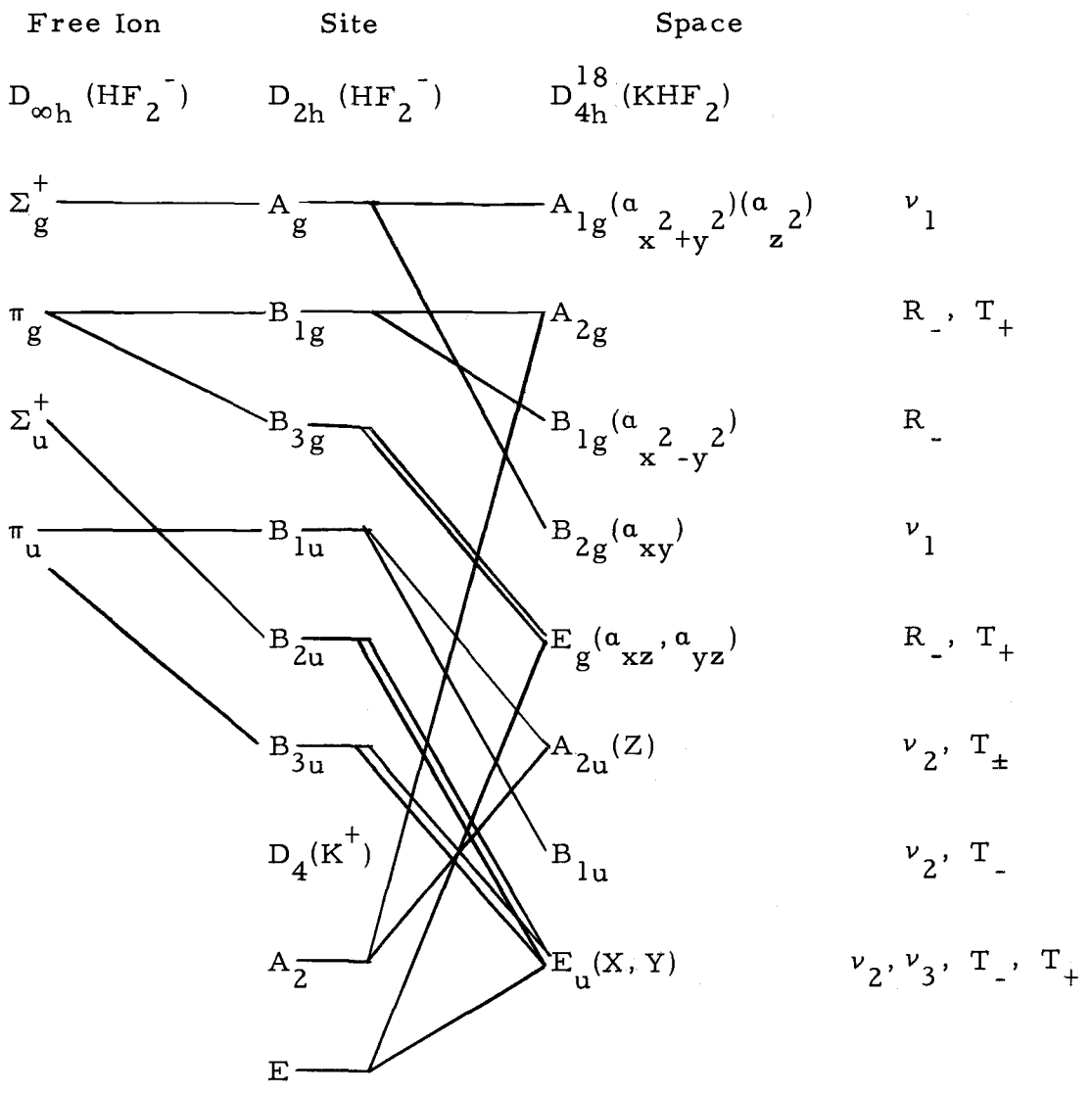

Figure I-4. Correlation diagram for KHF_2.

infrared-active if it belongs to a symmetry species A_{2u} or E_u. The Raman active modes include all the g species in the correlation diagram (i.e., the mode is positive to the center of inversion operation), except for the A_{2g} in the KHF_2 case. This will be discussed further in each of the respective infrared and Raman chapters.

Preparation

Both $NaHF_2$ and KHF_2 were purchased commercially with a purity of 98 percent and were recrystallized several times with distilled water. The bifluoride ion behaves chemically in a similar way to a solution of hydrofluoric acid, so certain precautions were necessary. Plastic polypropylene bottles were rinsed with a reagent-grade hydrofluoric acid (48 percent) solution and were used for all recrystallizational procedures as well as for storage containers. Both bifluoride salts were also prepared by the method described by Ibers and McGaw (3). This method involves slowly adding either sodium or potassium carbonate to a boiling solution of hydrofluoric acid.

$$4\ HF + M_2CO_3 \rightarrow 2\ MHF_2 + CO_2\uparrow + H_2O$$

$$M = Na \text{ or } K$$

However, this method did not noticeably increase the purity of the salts and since the preparation is hazardous as well as having the possibility of yielding polymeric species, MH_2F_3, the commercial

salts were used extensively.

Single crystals of KHF_2 can be obtained easily by either slow evaporation at constant temperature or by slowly lowering the temperature of a saturated solution. Both methods yield approximately the same quality of single crystal; however, the temperature gradient method produced larger crystals. These crystals were large enough so that seeding of the crystal was not necessary for the Raman and reflection experiments.

This method of slowly decreasing the temperature was accomplished by placing approximately 150 ml of a saturated solution of KHF_2 at 335°K into a plastic poly-bottle. This in turn was placed in a constant-temperature water bath at 340°K; then, after approximately one hour, the poly-bottle was covered and the water bath was turned off. When the bath reached room temperature the poly-bottle was taken out and the solution remaining was decanted off. The crystal size varied, but a typical size obtained was 15 mm x 15 mm x 1 mm thick. Larger crystals were grown by this same technique if a larger volume of the saturated solution was used. However, these were more irregular around the edges and had to be cleaved.

Small crystals (approximately 7 mm on a side) look like a tetragonal bipyramid with the two unique vertices cut off (shown below). Larger crystals appeared to be a thin slab with many edges. These edges were either at 45° or 90° to each other. This growth pattern is

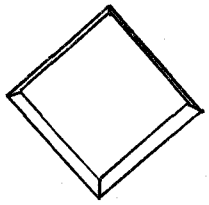

General View

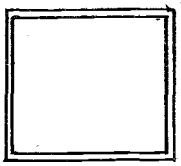

Top View

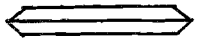

Side View

identical to the azide salt of potassium. The axes of these crystals were labeled to be referenced below in the Raman experiment.

Many attempts were made to grow the sodium counterpart with standard techniques. However, none of these were successful. Well oriented polycrystalline crystals of $NaHF_2$ were obtained by a slow evaporation technique inside a dry bag. A saturated solution with a volume of 150 ml in a poly-bottle was placed in a dry bag for several days. This was carried out at room temperature (~300°K), and the dry bag was flushed with dry N_2 four times a day. After a few days oval or elliptical rough-edged crystals were formed. The solution was decanted and the crystals were placed in a desiccator. All was accomplished in the dry bag. Polycrystals grown in this manner were 0.1 mm thick and have an area of approximately 100 mm^2. These crystals were noticeably not single, because of the pits and erratic breaks in the crystal (shown below). It will be established later in

Looking down the Z (optic) axis

reflection studies that the Z axis is perpendicular to the polycrystalline slab and in this way, it is well-oriented.

The deuterated analogs of $NaHF_2$ and KHF_2 were obtained by recrystallizing the respective salt from D_2O. The heavy water used was stated to have a purity of 99.8 percent. This was accomplished

$$D_2O + HF_2^- \rightleftharpoons DOH + DF_2^-$$

by placing a small 30 ml polypropylene bottle containing about 2.8 g of the salt (KHF_2 or $NaHF_2$) dissolved in 10 ml of D_2O in a glass vessel which in turn was connected to the vacuum line. The mostly deuterated water was pulled out with a liquid N_2 trap, leaving the partially deuterated salt. This deuteration process had to be performed several times in order to obtain a sample of 95 percent DF_2^-. After each deuteration, an infrared spectrum was taken to check the percent deuterium in the sample. The sampling and preparation of the DF_2^- were carried out in a dry bag, because the bifluoride ion exchanges very rapidly with water (moisture).

The equilibrium constant for the reaction given above was found experimentally to lie largely in the direction of HF_2^-, although an K_{eq} was not determined. The gas phase equilibrium constant was calculated by statistical thermodynamics and was 0.6 ($= K_{eq}$), which does not explain why many deuterations were required in order to obtain a sample of 95 percent DF_2^-. The D:H ratio of each deuteration

process was at least 20:1. For this reason, single crystals of KDF_2 or polycrystals of $NaDF_2$ were not of high enough purity or large enough to obtain reflectivity measurements.

Sampling Technique

In order to observe the amount of dipolar coupling in KHF_2 and $NaHF_2$, the effective crystal field must be kept the same throughout the entire experiment. This means the sites and the crystal structure of the two isotopic species should be the same. This can be accomplished by using either thin films or mulls. The Nujol mull technique was employed as the sampling method for these crystals, as it has two major advantages over the thin film technique. First, it would be extremely difficult to obtain a thin film of either $KH(D)F_2$ or $NaH(D)F_2$ with a thickness much less than the wavelength of light, approximately 8 μ. Secondly, mulls are convenient as well as easy to handle. The disadvantage of the mull technique is a solvent effect that would shift the frequency slightly. There are other disadvantages associated with both techniques, but these effect the spectra about the same.

In using the mull technique, one does not really observe the transverse frequency associated with the vibrational mode in the infrared, but normally a frequency that lies between the transverse and the longitudinal one. However, one can observe a shift in

frequency and/or a change in the intensity of the band.

Mulls of the bifluoride salts ($H(D)F_2^-$) were made in a dry bag by placing approximately 15 mg of the salt in a mortar, then grinding the salt for about 10 minutes. The particle size after grinding varied from 0.1 μ to 5 μ. Following this, one drop of high quality mineral oil was added to the mortar and ground for an additional five minutes. A rubber policeman was used to smear the mull onto two NaCl windows. The windows were then pressed together and placed in a holder for the infrared instrument.

Two infrared instruments were used for the study of infrared transmission as well as infrared reflectivity measurements of $NaH(D)F_2$ and $KH(D)F_2$. Both spectrophotometers are capable of high resolution; however, due to the large breadth or half-widths of the bands studied, it was not found necessary to operate the instruments with a resolution of less than 2 cm^{-1}. All of the $NaH(D)F_2$ infrared transmission and reflection spectra were taken on a Beckman I.R.-7; while most of the $KH(D)F_2$ spectra were taken on a Perkin Elmer-180. The reason for the change was that polarization studies could easily be performed on the P.E.-180, which has a built-in polarizer.

The infrared transmission and reflection spectra were taken in the double beam mode on both instruments. This almost completely eliminated the atmospheric absorptions when the purging system was operating well. However, due to a longer path length through the

sample compartment when taking reflection spectra, water vapor and carbon dioxide peaks were noticed. These absorptions did not affect the measurements in the ν_2 region of both crystals. Both instruments were calibrated, and the frequencies reported here have been corrected according to this calibration.

The Beckman IR-7 is a fore-prism/grating spectrophotometer, with the prism used for separating the orders of the grating. A Nernst glower is the light source and a thermocouple is used for the detector. Spectral band width (resolution) of 1 cm^{-1} can be achieved from 650 cm^{-1} to 4000 cm^{-1} without appreciable noise.

The Perkin Elmer-180 is a double-beam ratio-recording spectrophotometer with a range of 180 cm^{-1} to 4200 cm^{-1}, which is covered by a set of five gratings. An air-cooled globar is the source of radiation, and a thermopile is used as the detector. Spectral band widths of less than 1 cm^{-1} can easily be obtained, and a polarizer can be inserted in either the parallel or the perpendicular position for polarization studies.

II. INFRARED OBSERVATIONS

According to the correlation diagrams given on pages 7 and 9 for $NaH(D)F_2$ and $KH(D)F_2$, there are four active fundamental vibrations in the infrared spectrum for $NaH(D)F_2$ and six for $KH(D)F_2$. A brief treatment of the lattice region of each salt will be given, followed by a discussion of the internal vibrations.

Two of the four active vibrations of $NaH(D)F_2$ are of the internal type, $\nu_2(E_u)$ and $\nu_3(A_{2u})$, which involve internal vibration of the $H(D)F_2^-$ species only. The other two, $T_\pm(A_{2u})$ and $T_\pm(E_u)$, involve translations of both the Na^+ and the $H(D)F_2^-$. Only one of these two lattice vibrations has been observed in the infrared. P. Giguere and K. Sathianandan concluded from their far-infrared study that the two allowed translatory lattice vibrations are either accidentally degenerate or have a significant band overlap in frequency so that one only observes one band at 226 cm^{-1} (Table II-1) (11). This frequency of 226 cm^{-1} agrees quite well with the work of Rush, Schroeder, and Melveger in the far infrared (8). RSM reported a frequency of 228 cm^{-1} as well as a value of 180 cm^{-1} for the missing infrared band from their neutron inelastic scattering experiments. However, in their neutron scattering experiments, they did not observe the 228 cm^{-1} band which they saw in the infrared. This frequency of 180 cm^{-1} in the neutron time-of-flight spectra was a shoulder of a

strong 150 cm^{-1} band.

Table II-1. Lattice frequencies of $NaHF_2$ and $KH(D)F_2$.

Vibration	$NaHF_2$	$NaDF_2$
$T_{\pm}(A_{2u})$	226 cm^{-1} [a]	---
$T_{\pm}(E_u)$		

Vibration	KHF_2		KDF_2
$T_{\pm}A_{2u}$		146 cm^{-1} [b]	
$T_{\pm}E_u$	178 cm^{-1}, [a]	174 cm^{-1} [b]	174 cm^{-1} [a]
$T_{-}E_u$	130 cm^{-1}, [a]	130 cm^{-1} [b]	132 cm^{-1} [a]

[a] Obtained from Reference 11.

[b] Obtained from Reference 13 reflectivity measurements.

There are three lattice vibrations for the potassium salt, $T_{\pm}(A_{2u})$, $T_{\pm}(E_u)$, and $T_{-}(E_u)$, as well as three active internal vibrations, $\nu_2(A_{2u})$, $\nu_2(E_u)$, and $\nu_3(E_u)$. P. Giguere and K. Sathianandan also studied the lattice vibrations of the potassium salt (11). They observed only two vibrational bands in their far-infrared study, so they concluded that the missing vibrational band is accidentally degenerate, like that of the sodium salt. The frequencies of these lattice vibrations are 130 cm^{-1} and 178 cm^{-1} (132 cm^{-1} and 174 cm^{-1} for the deuterium-substituted species) for KHF_2 and were assigned $T_{-}(E_u)$ and both $T_{\pm}(A_{2u})$ and $T_{\pm}(E_u)$, respectively (Table II-1).

P. Giguere's and K. Sathianandan's samples were made by

evaporating a solution of the bifluoride salt on a polyethylene window. However, they stated that a pressed disk technique with polyethylene gave similar results. An unusual feature of the potassium salt is the shift to higher frequency of the $T_-(E_u)$ lattice vibration from 130 cm^{-1} to 132 cm^{-1} upon deuterium substitution.

G.R. Wilkinson calculated the imaginary part of the dielectric constant (ϵ'') from polarized reflectivity measurements of KHF_2 and plotted ϵ'' against frequency (ν) (13). He observed three maxima in the ϵ'' and these corresponded to frequencies of 130 cm^{-1}, 146 cm^{-1}, and 174 cm^{-1}. These were assigned to $T(E_u)$, $T_\pm(A_{2u})$, and $T(E_u)$ respectively. These frequencies should correspond to the transverse mode of the respective lattice vibration and Wilkinson made no attempt to distinguish between the two E_u modes, $T_\pm(E_u)$ and $T_-(E_u)$. His reflectivity measurements of single crystal KHF_2 could distinguish between the A_{2u} mode and the E_u modes, but it can not distinguish between two E_u modes.

The internal vibrations of $NaH(D)F_2$ and $KH(D)F_2$ have been extensively studied by several researchers (8, 10, 11, 12). It is now well established that there are two active internal vibrations for $NaH(D)F_2$ --$\nu_2(E_u)$ and $\nu_3(A_{2u})$--and three for $KH(D)F_2$--$\nu_2(A_{2u})$, $\nu_2(E_u)$, and $\nu_3(E_u)$. Since there are certain similarities between the spectra of $NaH(D)F_2$ and $KH(D)F_2$, some general comments about the ν_2 and ν_3 vibrational spectra of the pure species will follow.

A noticeable characteristic of the internal vibrations is the breadth of the absorption bands in the infrared. The widths at half height of ν_3 and ν_2 are ~450 cm^{-1} and 150 cm^{-1}, respectively, at room temperature (18). This broading associated with ν_2 and, especially, ν_3 of both salts cannot be explained entirely by the superposition of "hot" bands, since cooling the sample down to 77°K has a small effect on the half-widths (18). Salthouse and Waddington measured the half-widths of the potassium salt at 77°K and found that the half-widths of ν_3 and ν_2's were 360 cm^{-1} and 130 cm^{-1}, respectively. Even after cooling the sample down to 4°K, no appreciable decrease from the 77°K case was noticed. Intermolecular coupling of the bifluoride ions in the pure crystal was proposed as the source of these extreme half-widths. This explanation was based on their study of KHF_2 (2 percent) in KCl. This matrix-isolation experiment was first performed by Ketelaar, Haas, van der Elsken; however, Ketelaar and coworkers in their 0.02 percent KHF_2 study only observed a singlet for the ν_2 and ν_3 fundamentals (19). Salthouse and Waddington observed a shoulder with their concentrated matrix-isolation technique and attributed this shoulder to the formation of dimers (bifluoride ions on adjacent sites).

An electrostatic coupling scheme was employed for this dimerization. An infinite secular determinant was constructed for the pure crystal, while a two x two secular determinant was set up for the

dimeric case. An approximate solution for the dimeric case is shown below,

$$\nu = \nu_0 \pm \frac{e^2 f_{12}}{8\pi^2 m_H V_0 r_{12}^3} = \nu_0 \pm f(e, f_{12}, m_H, r_{12}) \qquad (I\text{-}1)$$

where ν represents the frequencies observed; ν_0, the unperturbed frequency; e, the effective moving field; f_{12}, the interaction constant; and r_{12}, the distance between the dimers. From this simple solution, the infinite solution was postulated leading to an infinite number of frequencies around the unperturbed frequency, ν_0; and the breadth would be determined by the $f(e, f_{12}, m_H, r_{12})$. Salthouse and Waddington pointed out that for a vibration, which depends primarily on the motion of the hydrogen, the $f(e, f_{12}, m_H, r_{12})$ is quite large.

In effect the foregoing theory is a dipolar coupling theory which has been described more generally elsewhere (15). There are a number of difficulties with Salthouse and Waddington model; 1) In a real three dimensional crystal, the summation of the coupling terms must be carried out with care about the convergence as we have taken in evaluating the S matrix elements; 2) Only the $K = 0$ modes are allowed, at least in a large harmonic crystal, so the Salthouse and Waddington model does not account for the breadth which is more properly described as the consequence of combined reflection and

absorption losses extending over the range from ν_T to ν_L.

The half-widths reported for ν_2 and ν_3 are the widths at half height for the nujol mull spectrum. Wilkinson observed a half-width of 40 cm^{-1} for the ν_3 fundamental of KHF_2; however, this was taken from his imaginary dielectric constant spectrum (13). The imaginary dielectric constant (ϵ'') was calculated from reflectivity measurements which were taken over the entire infrared region.

Another striking feature of the bifluoride ion is the anharmonicity that is associated with the ν_3 fundamental. Ketelaar observed a band at 5099 cm^{-1} and assigned it to the second overtone of ν_3 ($3\nu_3$) (20). This assignment was confirmed by Ketelaar and Vedder and by Cote and Thompson (12, 21). The second overtone of ν_3 for KDF_2 appears at 3561 cm^{-1}. If one simply multiplies the frequency of the corresponding ν_3 band by three, the bands should appear at 4350 cm^{-1} and 3069 cm^{-1} for the $3\nu_3$'s of the KHF_2 and KDF_2, respectively, using values of 1450 cm^{-1} for ν_3 of KHF_2 and 1023 cm^{-1} for KDF_2. This anharmonicity is extremely large, 749 cm^{-1} and 492 cm^{-1}, and is opposite in sign to the usual effect observed in diatomic molecules.

This apparently large negative anharmonicity was first explained by Pitzer and Westrum by a quartic term in the potential energy (22). Ibers later calculated the force constants of KHF_2 by assuming a quartic term in ν_3 and an interaction term involving both ν_3 and ν_1 (4). This potential energy scheme is shown below, where

$$2V = \frac{K_1}{\mu_1} Q_1^2 + \frac{K_3}{\mu_3} Q_3^2 + \frac{K_4}{\mu_3^2} Q_3^4 + \frac{K_{13}}{\mu_1^{1/2} \mu_3} Q_1 Q_3^2 \qquad \text{(I-2)}$$

the K's are the respective force or interaction constants, the Q's the normal coordinates, and the μ's the reduced masses of the respective modes. Ibers also included in his refinements,

$$\Delta = 0.0024 \text{ Å} = \langle \text{F-H-F} \rangle - \langle \text{F-D-F} \rangle , \qquad \text{(I-3)}$$

which is the maximum difference set by Ubbelohde (6). The inclusion of the $Q_1 Q_3^2$ term and the exclusion of the term $Q_1^2 Q_3^2$ in the potential energy comes about because the bond distances of <F-H-F> and <F-D-F> were taken to be different (Δ).

The result of Ibers' calculation showed that the quartic term Q_3^4 was approximately 15 percent of the quadratic (harmonic) term Q_3^2, while Pitzer and Westrum stated that the levels approach the levels of an oscillator with a fourth power potential (Q_3^4).

Polycrystalline Spectra

Nujol mull spectra were taken of each sample with various percent deuterium in the respective bifluoride salts. The range of deuteration varied from approximately three percent to 95 percent depending upon the salt. Before the discussion of these spectra, some terms will be defined and the correlation diagrams discussed more completely.

A coupled vibrational frequency is the frequency associated with the pure species. An example of this is the $\nu_2(E_u)$ mode for $NaHF_2$ with very little deuterium present (less than 5 percent). A decoupled vibrational frequency, on the other hand, is the frequency associated with the isotopic dilute species. An example of this type is the $\nu_2(E_u)$ mode for $NaHF_2$ with a high percent deuterium present in the sample (greater than 90 percent). As a final point, one should consider how the correlation diagram changes for the isotopic dilute species. The space group (factor group) splittings no longer exist for the dilute species; however, the static crystal field perturbation does exist, so the site symmetry column (Chapter I) shows the activity of the vibrational mode. An example of this is the correlation diagram for the bending vibration ν_2 of the potassium salt. The $\nu_2(B_{1u})$ and $\nu_2(B_{3u})$ modes of HF_2^- would be the symmetry of the bending vibrations for the dilute HF_2^- species. In other words, the site symmetry must be considered in order to see the activity and the symmetry of the vibrational mode in question. Since the factor group and the site group are the same for $NaHF_2$, the symmetries (and the activities) of the vibrational modes are the same.

Because of the difficulty in assigning a frequency to the ν_3 band and other complications that will be discussed later, this study has been concentrated upon the ν_2 bands. The results of the $NaH(D)F_2$ system will be discussed first.

Rush, Schroeder, and Melveger studied the bifluoride system using the same technique and their results are tabulated in Table II-2. Their isotopic substitution percentages range from two percent to 80 percent deuterium, while the results in this study range from three percent to 96 percent. The percent deuterium in our samples was determined by the area of the absorption-vs-frequency plot of both ν_2 band of the hydrogen as well as the deuterium species in the sample. The mass difference of the two species must be corrected in using this technique, because the amplitude of vibration for the hydrogen species is roughly twice that of the deuterium species. The amplitude of the $\nu_2(HF_2^-)$ mode, using the G matrix element for the vibrational mode for ν_2, is 1.95 that of the $\nu_2(DF_2^-)$.

Spectra of the ν_2 regions of $NaHF_2$ and $NaDF_2$ with various percent deuterium substitutions are shown in Figure II-1. The right side of the drawing is the ν_2 region of $NaDF_2$, while the left is the ν_2 region of $NaHF_2$. The frequencies of the coupled bending vibrations of $NaHF_2$ and $NaDF_2$ were found at 1211 cm^{-1} and 874 cm^{-1}, respectively. This is shown by the lower left drawing and the upper right drawing in Figure II-1. These frequencies correspond essentially with the pure nujol mull spectra of either $NaHF_2$ (98 percent) and $NaDF_2$ (96 percent). Consider only the right hand side of Figure II-1 which is the bending region for the ν_2 mode of $NaDF_2$. The pure, approximately 96 percent, $NaDF_2$ has a maximum absorption at

Table II-2. Internal bending vibrational frequencies for $NaH(D)F_2$ and $KH(D)F_2$.

Mode	Present Assignment (cm^{-1})	Previous Assignment (cm^{-1})
$\underline{NaHF_2}$		
$\nu_2(E_u)$ DF_2^- (coupled)	874	874[a]
HF_2^- (coupled)	1211	1210[a]
$\nu_2(E_u)$ DF_2^- (uncoupled)	893	893[a]
HF_2^- (uncoupled)	1240	--
$\underline{KHF_2}$		
$\nu_2(A_{2u})$ DF_2^- (coupled)	890	891[b]
$\nu_2(E_u)$ DF_2^- (coupled)		
$\nu_2(A_{2u})$ HF_2^- (coupled)	1214 (1233 sh.)	1233 (b.c.)[a]
$\nu_2(E_u)$ HF_2^- (coupled)		
$\nu_2(B_{1u})$ DF_2^- (uncoupled A_{2u})	911	912[a]
$\nu_2(B_{3u})$ DF_2^- (uncoupled E_u)	894	895.5[a]
$\nu_2(B_{1u})$ HF_2^- (uncoupled A_{2u})	1263	--
$\nu_2(B_{3u})$ HF_2^- (uncoupled E_{3u})	1238	--

[a] Reference 8.

[b] Reference 20.

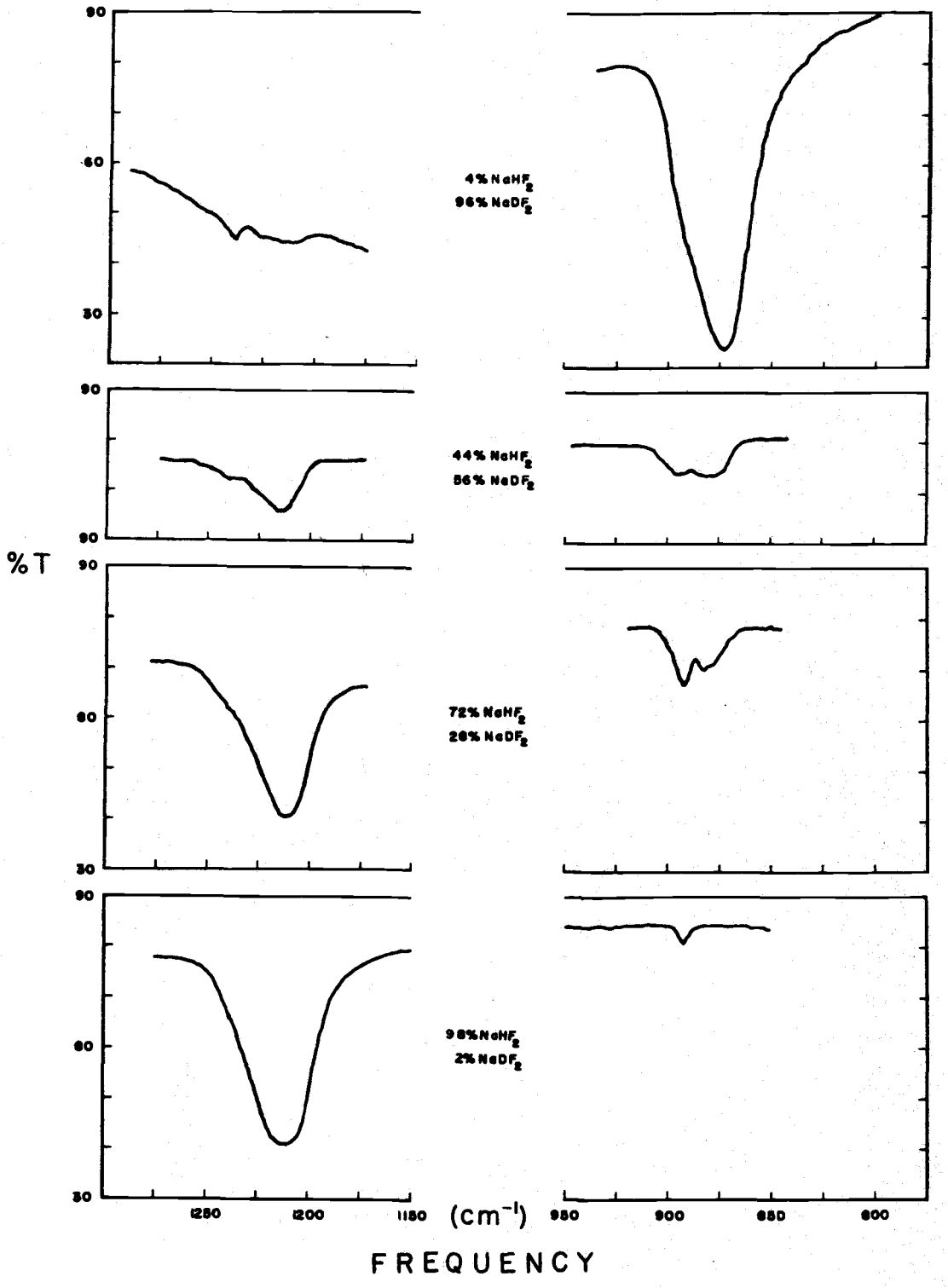
%T
90
60
30
4% NaHF2
96% NaDF2
44% NaHF2
56% NaDF2
72% NaHF2
28% NaDF2
98% NaHF2
2% NaDF2
1250
1200
1150
950
900
850
800
(cm⁻¹)
FREQUENCY

874 cm^{-1}, and as one increases the percent hydrogen in the sample the bending vibrational band shifts to higher frequency. This is indicated in the next drawing (56 percent DF_2^-) where a broad doublet appears. Then, increasing the hydrogen even more the band center of the doublet continues to shift to even a higher frequency (28 percent DF_2^-). Finally a single peak was observed for the two percent deuterated sample. The center of this peak is at 893 cm^{-1} and this should correspond to the uncoupled frequency of $NaDF_2$ in a $NaHF_2$ lattice. The same type of illustration is true for the left side (ν_2 of $NaHF_2$ region), but working up the left side instead of going down. The uncoupled frequency of $NaHF_2$ in $NaDF_2$ appears at 1240 cm^{-1} (upper left drawing in Figure II-1); however one notices a residual coupling between 1200 cm^{-1} and 1230 cm^{-1} for the $NaHF_2$ dilute case. This may well be caused by being slightly more concentrated than the corresponding dilute $NaDF_2$ case and/or by a larger dipole moment derivative $(\frac{\partial \mu}{\partial q})_0$ that is associated with the ν_2 of HF_2^- species compared to the ν_2 of the DF_2^- species. The ν_2 frequencies of $NaH(D)F_2$ we observed and those of RSM are listed in Table II-2.

The value of 893 cm^{-1} for the decoupled deuterium bifluoride of the sodium salt agrees with RMS result (8). RMS did not observe a frequency for the decoupled HF_2^-, because the percentage of deuterium in the sample was not high enough. As mentioned earlier the deuteration process was performed approximately 20 times to reach a

concentration of 96 percent $NaDF_2$.

Figure II-1 illustrates the principles of the isotopic dilution technique for $NaH(D)F_2$ where the crystal or static field around the dilute species is roughly the same as that around the pure salt. Also, the band-widths at half heights are considerably narrower for the uncoupled vibrational modes compared to the coupled vibrations. Now, the same principle will be presented for the potassium salt.

The bending region of the potassium salt is more complicated than that of the sodium salt, because there are two bending vibrations ($\nu_2(E_u)$ and $\nu_2(A_{2u})$) allowed in the infrared for KHF_2 and KDF_2. Since the frequencies of the coupled vibrational mode are very close together, it is difficult to separate the vibrational band into the two components for either the pure KHF_2 or KDF_2 by the nujol mull technique. However, Wilkinson separated the two components with reflectivity measurements and obtained through transformations a plot of the imaginary dielectric constant ϵ'' versus the frequency for the KHF_2 salt (13). He reported frequencies of 1227 cm^{-1} and 1234 cm^{-1} for $\nu_2(E_u)$ and $\nu_2(A_{2u})$, respectively. These frequencies are for the transverse optical phonon modes which may or may not agree with the infrared "absorption" spectrum. This will be discussed in more detail later in the text. In the infrared the values for the maximum absorption range from 1210 cm^{-1} to 1233 cm^{-1} for the ν_2 mode of KHF_2 (Table II-2) (8, 10). Ketellar reported an absorption maximum

of 891 cm^{-1} for the bending region of KDF_2 (10). RSM reported values of 895.5 cm^{-1} and 912 cm^{-1} for the decoupled frequencies of the ν_2 modes of KDF_2.

Spectra of the KHF_2 - KDF_2 system in various concentrations are shown in Figure II-2. The values of the coupled and the decoupled frequencies will be stated and the figure will not be discussed in the detail that the sodium salt was discussed. The upper right and the lower left drawings on Figure II-2 show the decoupled frequencies of both components and of both dilute species. Frequencies of 894 cm^{-1} and 911 cm^{-1} are assigned to the decoupled vibrational modes of the deuterium species and are assigned to the $\nu_2(B_{3u})$, $\nu_2(B_{1u})$, or uncoupled $\nu_2(E_u)$, $\nu_2(A_{2u})$, vibrational modes, respectively (Table II-2).

It was assumed that the uncoupled mode of $\nu_2(A_{2u}) > \nu_2(E_u)$, since the lower frequency band (894 cm^{-1}) of both dilute species is more intense than the higher frequency band (911 cm^{-1}). Later in the text, the inplane $(xy)(\frac{\partial \mu}{\partial q})_0$ is found to be larger than the out of plane $(z)(\frac{\partial \mu}{\partial q})_0$. This also is consistent for the dilute (HF_2^-) modes, since the 1238 cm^{-1} band is more intense than that of the 1263 cm^{-1} band. Similarly the decoupled vibrational frequencies of KHF_2 are 1238 cm^{-1} and 1263 cm^{-1}. These correspond to the uncoupled $\nu_2(E_u)$ and the uncoupled $\nu_2(A_{2u})$ modes, respectively. The uncoupled frequencies of this work as well as those of RSM are also given in Table II-2.

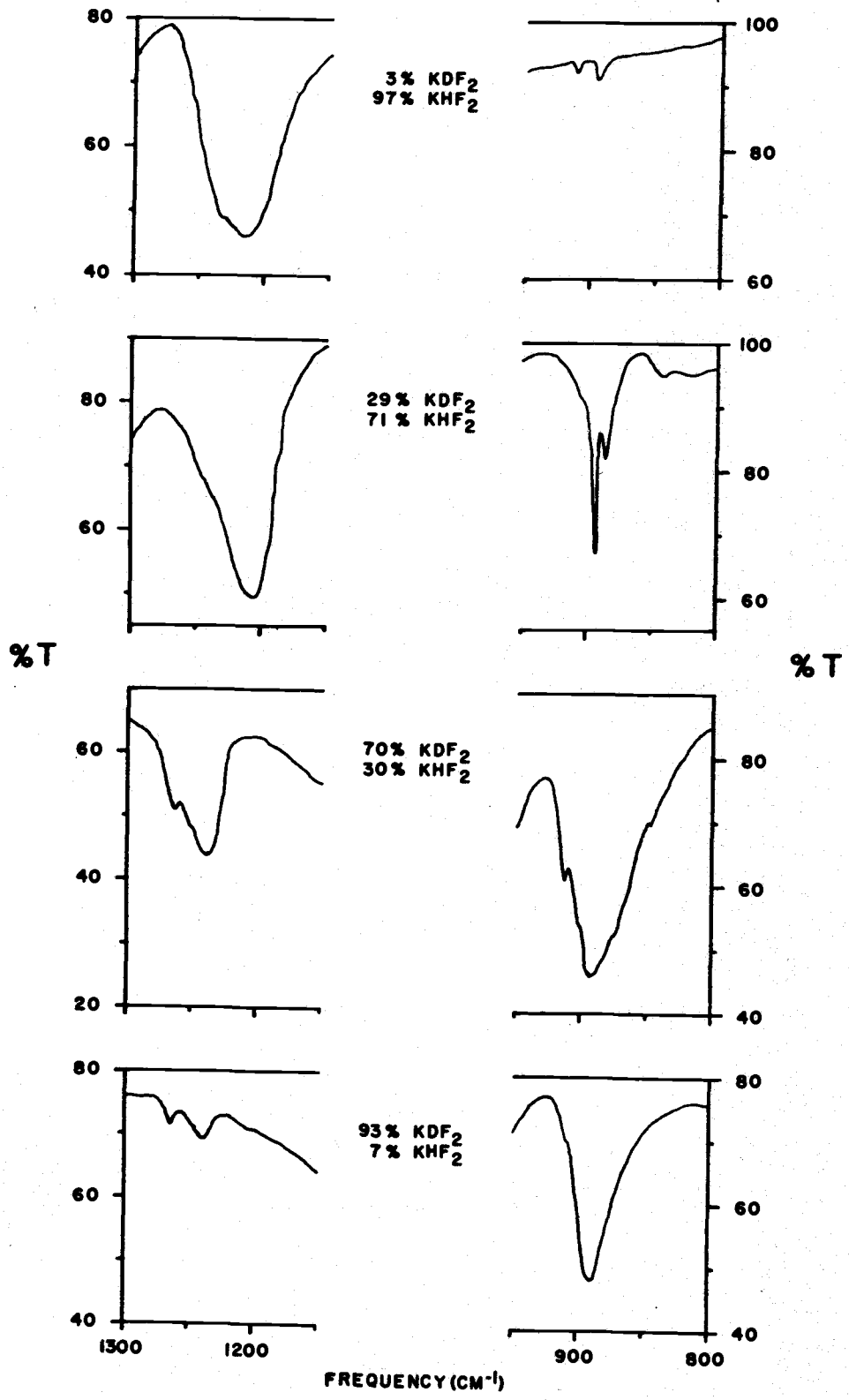
3% KDF2
97% KHF2
29% KDF2
71% KHF2
70% KDF2
30% KHF2
93% KDF2
7% KHF2
%T
%T
FREQUENCY (CM-1)
1300
1200
900
800

Values of the uncoupled frequencies for HF_2^- species were not obtained by RSM because the deuterium concentration was not high enough.

The coupled vibrational modes of both the KHF_2 and KDF_2 were not separable into their respective A_{2u} and E_u components (upper left and lower right drawings in Figure II-2). Frequencies of 890 cm^{-1} and 1214 cm^{-1} are given for the coupled bending vibrations of KDF_2 and KHF_2, respectively. A shoulder appears at 1233 cm^{-1} for KHF_2 and the center of the band is at 1225 cm^{-1}.

The isotopic ratios of the uncoupled as well as the coupled vibrations at $KH(D)F_2$ and $NaH(D)F_2$ is very close to that of a harmonic oscillator. Ratios of 1.388 were found for $NaH(D)F_2$ system, while the frequencies ratios of 1.385 were found for both $\nu_2(A_{2u})$ and $\nu_2(E_u)$ uncoupled vibrations. RSM value of 1233 cm^{-1} fits better (1.385) than our frequency of 1214 cm^{-1} (1.365); however RSM frequency is for the center of the absorption band, while the frequency that we report is that of maximum absorption.

III. REFLECTION SPECTRA

There are three degrees of freedom associated with an infrared-active vibrational mode (ν_i) of a solid. These are the transverse (ν_{iT}) and the longitudinal (ν_{iL}) phonon frequencies and are doubly and non-degenerate, respectively. When a wave propagates through a crystal, entire planes of atoms in the crystal (near the center of the Brillouin zone, K = 0) move in phase. If this motion is parallel to the propagation direction the wave is longitudinal and if it is perpendicular the wave is transverse. The discussion in this text will be limited to determining these frequencies only associated with the bending vibration. However, frequencies of the ν_3 band will be estimated in this chapter because ν_2 and ν_3 of both salts are within a few hundred cm^{-1}. The ν_3 mode was not analyzed because: (1) the partial quartic potential, (2) an unusual band width, (3) and possible combination bands in the same region of ν_3.

An electrostatic model was employed which has previously been treated by Born and Huang (23). When one applies an electromagnetic field to this crystal, the picture becomes more complex. The field interacts with the transverse phonon mode and breaks down the degeneracy, thus creating polaritons. This interaction takes place very close to the center of the Brillouin zone. Dispersion curves for both models are shown below. Throughout the remainder

of this text the values of the transverse and the longitudinal frequencies shall be understood as limiting values associated with the purely mechanical phonon modes.

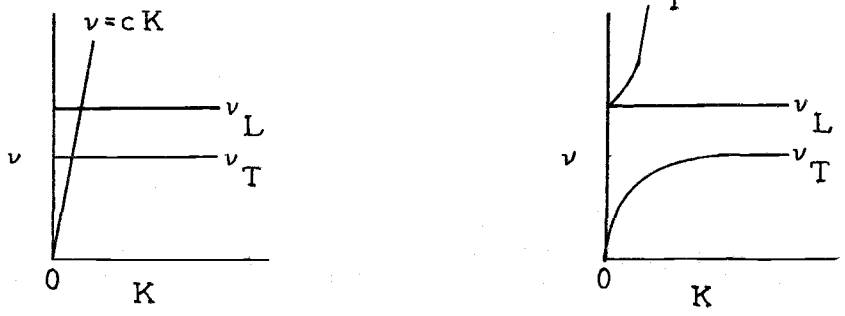

The transverse and the longitudinal frequencies associated with the bending vibrations of both salts can, in principle, be determined by a reflection spectrum. To aid in the assignment of these frequencies for each mode, a theoretical curve was compared to the experimental reflection spectrum. The comparison was made by eye rather than by a least squares method because of the number of experiments, number of parameters, and the weighting factors of each. Approximate values of ν_T and ν_L for each of the bending vibrations were obtained for both salts.

There are two basic types of reflection spectra that can be obtained from a crystal. In the R_E experiment, the electric field vector is perpendicular to the plane of incidence; while in the R_M experiment, the magnetic field vector is perpendicular to the plane of incidence (shown below). The reflection in both cases is related to

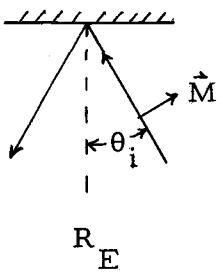

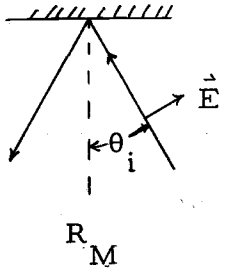

the refractive indices (n_i) and the angle of incidence, θ_i, as shown below in Equations (III-1) and (III-2), where θ is the propagation angle. This propagation angle θ can be obtained using Snell's equation in terms of n and θ_i. These equations for R_M and R_E are given for a x-y crystal face and the y-z as the plane of incidence, where $n_x^2 = \epsilon_x$, $n_y^2 = \epsilon_y$ and n which appears in the R_M expression is dependent upon the propagation direction in the crystal, $n^2 = \epsilon$ (Equation III-3).

$$R_E = \left| \frac{\cos\theta_i - n_x \cos\theta}{\cos\theta_i + n_x \cos\theta} \right|^2 \qquad \text{(III-1)}$$

$$R_M = \left| \frac{n_y^2 \cos\theta_i - n\cos\theta}{n_y^2 \cos\theta + n\cos\theta} \right|^2 \qquad \text{(III-2)}$$

Both equations are very cumbersome to work with since the refractive index, in general, has a real as well as an imaginary part (24). Therefore, a general description of these two types of reflectivities, as well as the properties involved, will be presented.

Maximum reflectivity occurs, for a crystal without damping, whenever the dielectric constant (real in this case) is negative, for a normal reflection frequency, ν, such that $\nu_T \leq \nu \leq \nu_L$. This can easily be seen via the behavior of the dielectric constant. So, one can inspect the dielectric constant instead of the individual R_E and R_M equations for an ideal crystal. Since this has been done by several authors for the near normal incident angle experiment, it will not be presented here (24). Also, the behavior of R_E with the angle of incidence different from zero ($\theta_i > 15$ degrees) is similar to the near normal case; it will also be omitted. However, the R_M case for θ_i different from zero will be presented because of its unique property.

In the following section, this discussion will be limited to the KHF_2 crystal; however, it may be applied to other uniaxial crystals. The X-Y face of KHF_2 and a nondegenerate vibrational mode (A_{2u}) will be considered. The activity or the dipole moment vector is in the Z direction for the A_{2u} species. The reflection experiment is shown below, where the polarization is indicated by the arrow perpendicular to the incoming radiation.

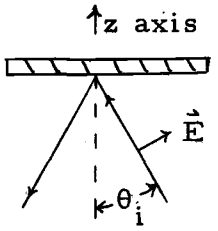

Applying Fresnel's equation to the T_M case described above, one obtains the relation

$$\epsilon_\theta = \frac{\epsilon_x \epsilon_z}{\epsilon_x \sin^2\theta + \epsilon_z \cos^2\theta} , \qquad \text{(III-3)}$$

where θ is the angle between the line of propagation of the wave going through the crystal and the Z-axis. Now, using Snell's law one can easily obtain

$$\epsilon_\theta = \epsilon_x - \left(\frac{\epsilon_x - \epsilon_z}{\epsilon_z}\right)\sin^2\theta_i . \qquad \text{(III-4)}$$

Now consider a case which there is dispersion only in the Z direction; then ϵ_x^0 can replace ϵ_x, and ϵ_z can be written, ignoring the damping constant, as

$$\epsilon_z = \epsilon_z^0\left(1 + \frac{\nu_L^2 - \nu_T^2}{\nu_T^2 - \nu^2}\right) . \qquad \text{(III-5)}$$

For simplicity, let $\epsilon_x^0 = \epsilon_z^0 = 1.0$ and solving for ϵ_θ in terms of ν_T, ν_L and ν, one arrives at

$$\epsilon_\theta = 1 + \frac{\nu_L^2 - \nu_T^2}{\nu_L^2 - \nu^2}(\sin^2\theta_i) . \qquad \text{(III-6)}$$

It can easily be seen from the above equation that the dielectric

constant is a negative quantity when $\nu_L < \nu < \nu_{LL}$, where ν_{LL} is defined by the equation

$$0 = 1 + \frac{\nu_L^2 - \nu_T^2}{\nu_L^2 - \nu_{LL}^2} \sin^2\theta_i \,. \qquad \text{(III-7)}$$

Thus for this particular reflection experiment, maximum reflectivity occurs at a frequency slightly above the longitudinal mode. Notice that this type of reflectivity increases with $\sin^2\theta_i$. This frequency above the longitudinal frequency (ν_{LL}) shall be called the quasi-longitudinal frequency. If one includes the damping constant and different ϵ_x^0 and ϵ_z^0, the expression is more complicated; however, the essential feature (ν_{LL}) remains intact.

The same phenomenon occurs for a degenerate vibration, provided the crystal face is chosen such that the optic axis is parallel to the plane of incidence and the interface is parallel to the optic axis (shown below). The reflecting face is the XZ plane, while the incidence plane is the YZ plane. The two arrangements of the optic axis, crystal face, and plane of incidence that would give a

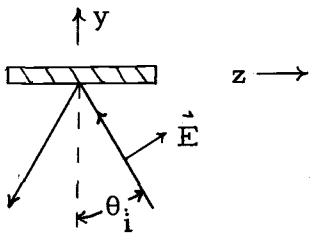

quasi-longitudinal reflection spectrum for a uniaxial crystal, were given above. Notice that this super longitudinal reflection occurs when the electric field vector has some component perpendicular to the crystal face and the other component can not be reflected by the same vibrational mode.

To illustrate this, consider the reflection arrangement possible for a uniaxial crystal, where the active vibrational mode is either in

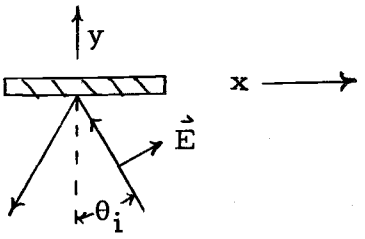

the X or the Y direction, E_u species. A quasi-longitudinal reflection for this E_u species will not occur because it has dispersion in the X as well as the Y direction. This can readily be seen by inspecting Fresnel's equation,

$$\epsilon_\theta = \frac{\epsilon_x \epsilon_y}{\epsilon_x \cos^2\theta + \epsilon_y \sin^2\theta} \qquad \text{(III-7)}$$

where $\epsilon_x = \epsilon_y$ for this degenerate vibration. Substituting $\epsilon_x = \epsilon_y$ into Equation III-7 one obtains

$$\epsilon_\theta = \epsilon_x = \epsilon_y .$$

Notice that ϵ has no angle dependence and a normal dispersion exists (i.e., similar to the other R_E and R_M experiments where the maximum reflectivity occurs between the longitudinal and the transverse frequencies).

This quasi-longitudinal reflection is generally weaker at low incident angles than the normal reflection spectrum of the same vibrational mode, because it depends on $\sin^2\theta_i$. The reflection work that will be presented in this chapter involves two different angles of incidence (10 degrees and 37 degrees). Since both $NaHF_2$ and KHF_2 are uniaxial, there are 12 possible different types of reflection experiments. Six of the 12 are either equivalent to the other six or would not contribute any additional information.

The theoretical curves for each of these experiments were obtained via a computer program.[1] The damping constants (Γ_i's), transverse and longitudinal frequencies for each vibrational mode in that region and the dielectric constants at infinite frequency for the crystal are the input to the program. Since the ν_3 mode is close to the ν_2 modes for both salts, approximate limits were set for the ν_3 vibration (13). The lattice vibrations were ignored since the frequencies are approximately 1000 cm^{-1} lower than the bending modes.

---

[1] I am indebted to Dr. R. Carlson and Dr. R. Frech for this program.

Once the parameters of the bending vibrations of both crystals were set, the transverse and longitudinal frequencies of the respective deuteriated salts were calculated using the ratio of the uncoupled frequencies. This was done since single or poly-crystals of either the sodium or the potassium salts did not contain sufficient deuterium bifluoride for reflection studies.

Ketelaar and Vedder studied KHF_2 by reflection spectroscopy and found that the maximum reflectivity occurs at 1238 cm^{-1} and 1245 cm^{-1} for the $\nu_2(E_u)$ and $\nu_2(A_{2u})$ vibrational modes, respectively (12). This was the first reflection spectra taken of KHF_2 and no attempt was made to determine the transverse and the longitudinal mode associated with each of these vibrations. Later, Wilkinson studied KHF_2 and through a transformation of his reflection spectrum to an imaginary dielectric constant spectrum, reported values of 1227 cm^{-1} and 1234 cm^{-1} for the transverse modes of the $\nu_2(E_u)$ and $\nu_2(A_{2u})$, respectively (13).

Two different angles of incidence were used in the present work for the reflectivity measurements of $NaHF_2$ and KHF_2. An angle of incidence of 10 degrees (near normal) was obtained by using a Perkin Elmer apparatus, shown in Figure III-1. The first mirror is flat so there is no additional convergence associated with this arrangement. The second mirror is where the crystal is placed. The crystals were placed on a cardboard with an opening cut out of the middle slightly

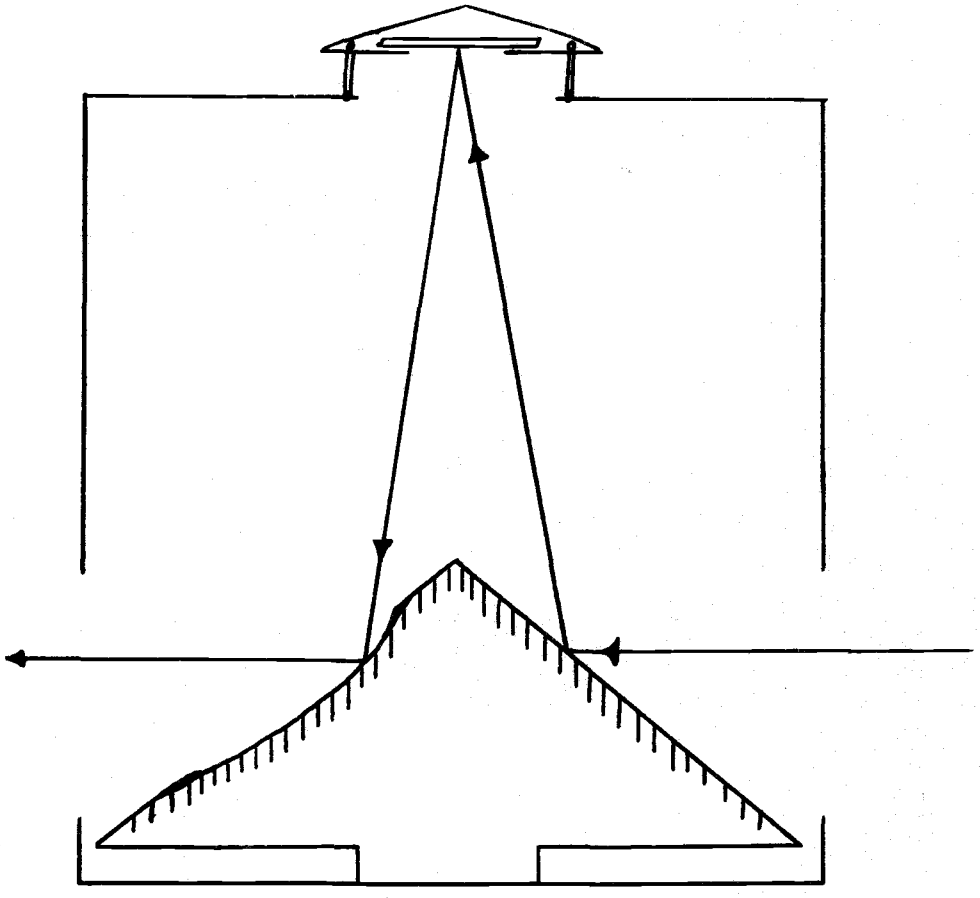

Figure III-1. Optics of the Perkin Elmer near normal (10 degrees) apparatus.

less than the size of the crystals. Then the cardboard was placed on top of the apparatus. The top of the apparatus is a tripod which can tilt or move the crystal. The last mirror is a convergent one, which makes a correction to the longer path that the light travels. This convergent mirror is necessary, since the light rays are convergent in both instruments. The only adjustment of this apparatus is the tripod located at the top.

An angle of 37 degrees was obtained by a Barnes beam condensor attachment, placing the crystal on a mount which replaced the flat mirror. The crystal was mounted with vacuum sealing putty. The flat mirror was masked to the size of the crystal and was used for setting 100 percent reflectivity of the sample. This arrangement is shown in Figure III-2, where the thick mirrors in the drawing represent convergent mirrors and the thin mirror is the flat mirror where the sample is placed. There is a larger error in the angle of incidence with this arrangement than with the near normal apparatus, because of the convergent mirrors before the sample. Each mirror can be tilted back and forth or rotated; therefore it is more difficult to maximize the single beam energy with this apparatus than with the near normal apparatus. The signal that one can expect is approximately 40 percent (IR-7) and 80 percent (PE-180) of the single beam energy without the attachment in the instrument; while with the 10 degree apparatus one should expect 25 percent for IR-7 and 35

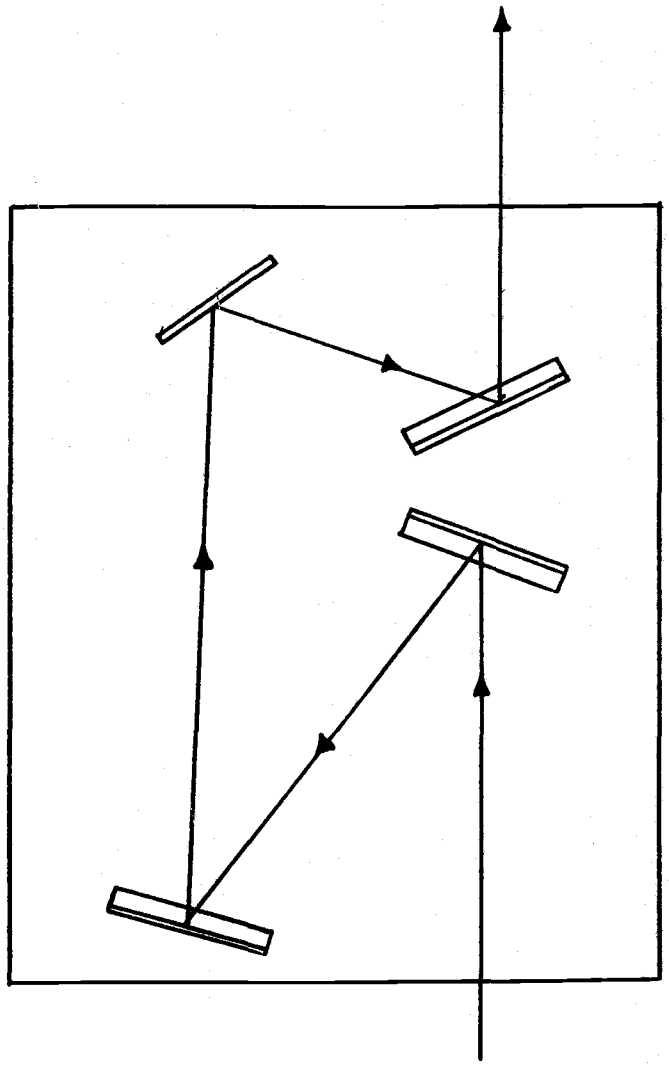

Figure III-2. Optics of the adapted Barns beam condensor (37 degrees).

percent for PE-180.

Both instruments were operated in the double beam mode. After placing a silver mirror in place of the sample, the 100 percent line was set where maximum reflectivity occurs in the bending region of the sample. The reflectivity of the silver mirror only varied by approximately two percent through the bending region (1200-1300 cm^{-1}). It was not necessary to correct for this slight fluctuation. Resolution is not a problem for reflectivity measurements because of the great width of the bands. Most of the reflection spectra were obtained with a spectral band width of less than two cm^{-1}. A Perkin-Elmer wire grid AgBr polarizer was used in both instruments.

Both instruments have a preferred polarization, i.e., the electric field vector in one direction has more intensity than the corresponding perpendicular direction. However, if a polarizer is placed in the instrument and the 100 percent reflectivity line is adjusted for each polarization, one can treat the instrument as not having any preferred polarization. All the reflection spectra that will be shown are polarized, so the instrument polarization is small. Also, in both instruments, the beam is converged through the sample area. This contributes an error to the angle of incidence in the reflection spectra. This error is larger (more convergences) for the PE-180 than the IR-7. Therefore, one does not observe 10 degrees or 37 degree reflection spectrum, but a range centered around these

angles. This is very difficult to estimate, since there is more light passing through the center of the beam than the perimeter of the beam (larger convergent angles). This error decreases in magnitude, since the crystal is smaller than the beam, so the center rays (more intense) would strike the crystal.

Reflection spectra were obtained of the well oriented poly-crystalline $NaHF_2$ at 37 degrees as well as 10 degrees. The $NaHF_2$ crystals grow in a thin sheet with the optic (Z) axis perpendicular to the sheet. Therefore, only reflection spectra were obtained on the X-Y face. The bending vibration belongs to the E_u symmetry species, so the quasi-longitudinal reflection was not observed for ν_2. Since the R_M experiment would not differ much from the R_E experiment, only the results of the R_E reflection spectra will be shown. The 100 percent reflectivity does not mean as much for the $NaHF_2$ because of the pitted nature of the well oriented poly-crystal. Also, one would not expect as high a reflectivity as for a single crystal.

The reflection spectra for $NaHF_2$ are shown in Figures III-3 and III-4 for the 10 degree and 37 degree R_E experiments. Also, shown are the theoretical curves for $NaHF_2$. Because the optical quality of the crystal surface was not very good, the absolute reflectivity obtained is not meaningful and one can understand why the experimental peak reflectivity is rather low, particularly with the apparatus used for the 10 degree measurement which requires a

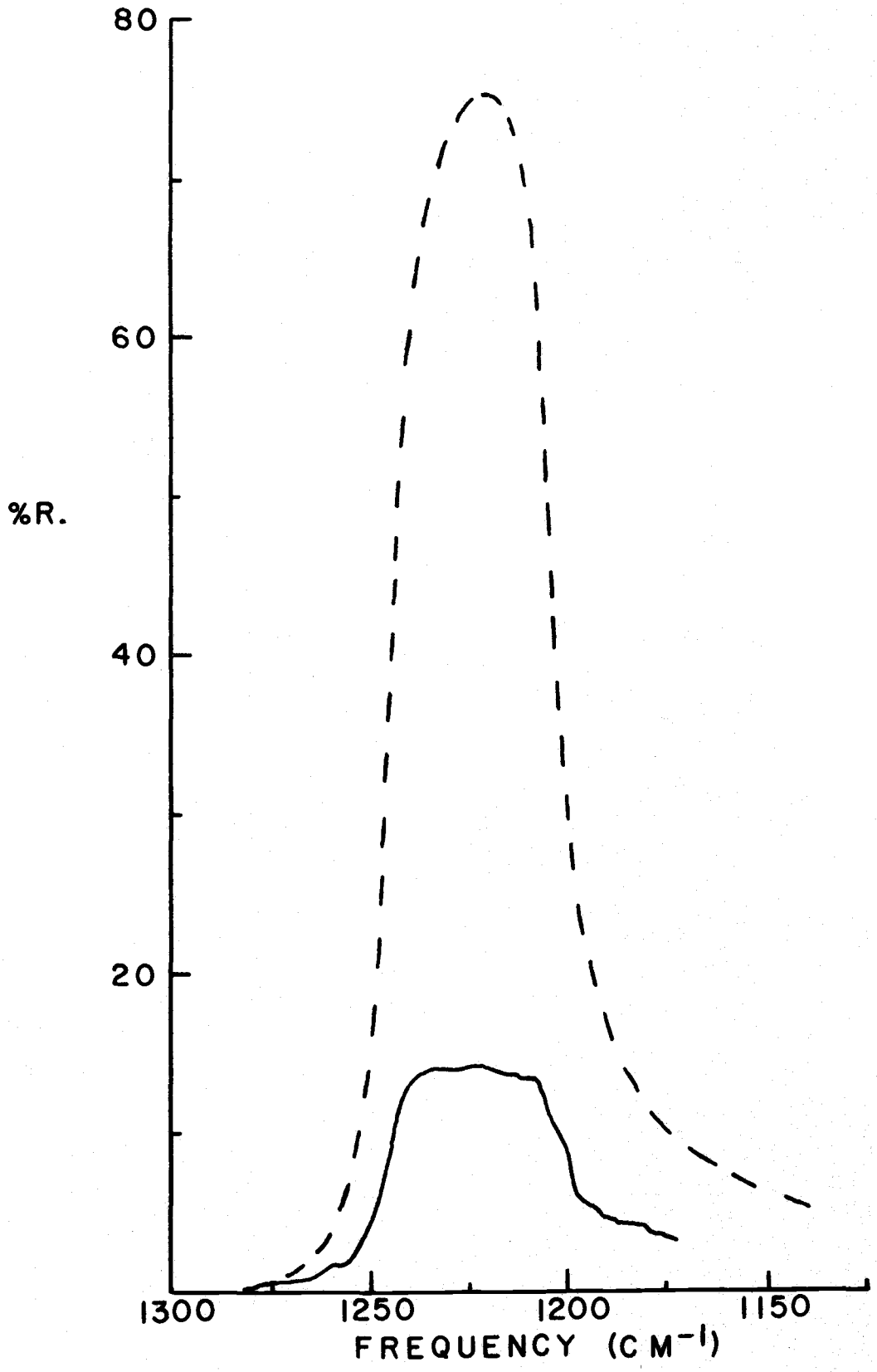
80
60
40
20
%R.
1300
1250
1200
1150
FREQUENCY (C M⁻¹)

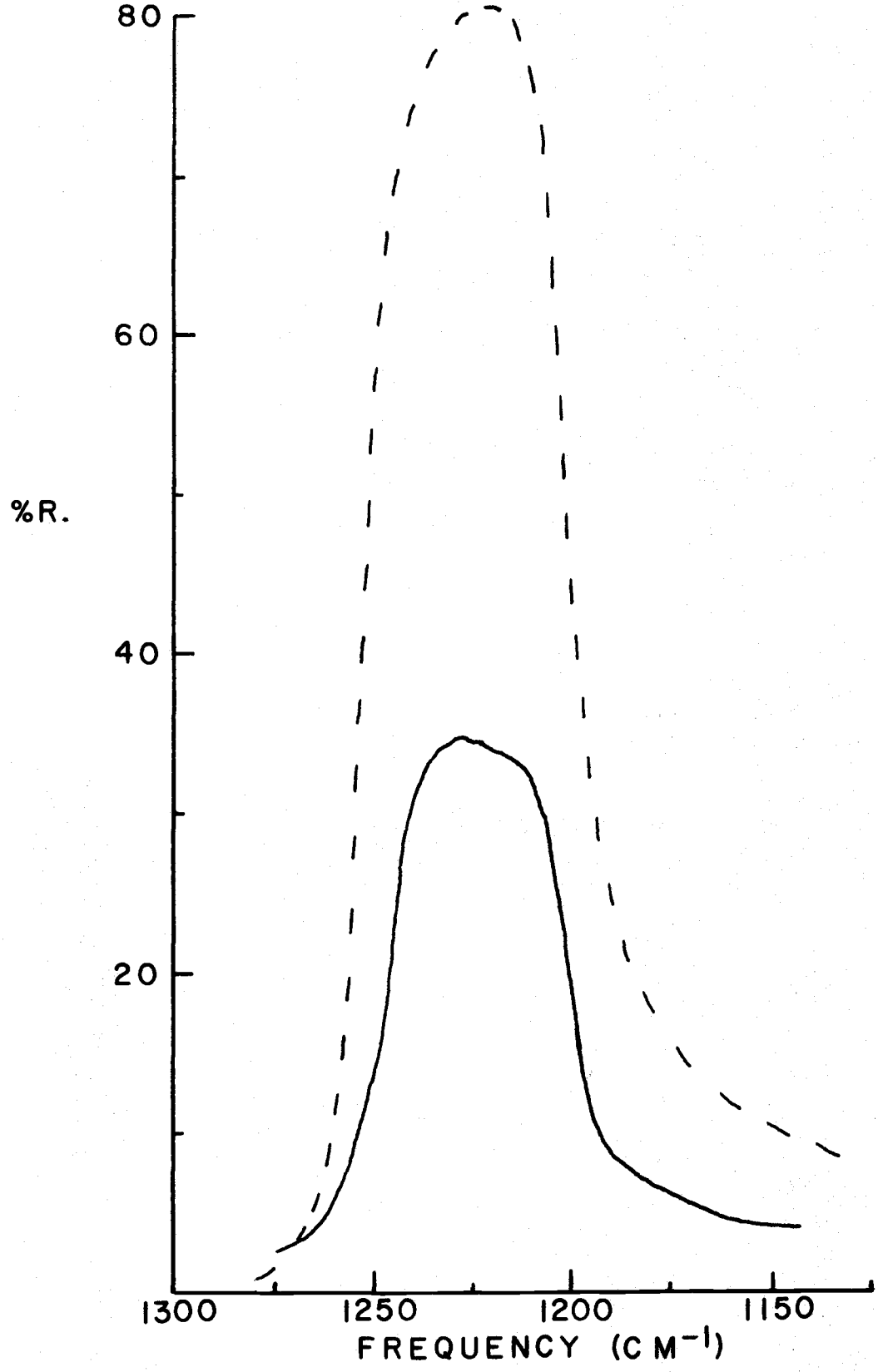
80
60
40
20
%R.
1300
1250
1200
1150
FREQUENCY (C M⁻¹)

larger surface area. It was therefore necessary to choose the parameters of the theoretical reflectivity to fit the shape but not the magnitude of the experimental curve. This was done by fixing $\epsilon_x(\infty) = 1.5901$, $\epsilon_z(\infty) = 1.7636$, and varying Γ, ν_T, and ν_L. The damping constant was varied from 0 to 18 cm^{-1} and was then fixed at 6 cm^{-1} with an estimated error of 3 cm^{-1}, and ν_T and ν_L were adjusted as follows. The ν_T and ν_L were estimated to occur at 4/5 of the maximum reflectivity, then these values were imput into the theoretical reflection curve. The theoretical ratio of the transverse and longitudinal frequencies were determined from the output. These ratios were compared to the experimental ratios and then new ν_T and ν_L values were input into the computer. This was done several times until a reasonable fit of the ratios were found for both angles of incidence. The experiment ratio for the longitudinal ratio is higher for the 10 degree case (lower for the 37 degree experiment) than the theoretical ratio, while the transverse ratios are very close (Table III-1). Increasing the longitudinal frequency, one would obtain a better ratio fit to the 10 degree experiment, but a poorer fit to the 37 degree experiment. The transverse limit was set at 1206 cm^{-1} while the longitudinal frequency corresponds to 1244 cm^{-1}. All the damping constant does theoretically is broaden or sharpen the reflection curve. Values of 1520 cm^{-1}, 1650 cm^{-1} and 15.0 cm^{-1} of ν_T, ν_L, and Γ respectively were used for the $\nu_3(A_{2u})$ vibration. It was

not critical in estimating these values since the two vibrational modes are of a different symmetry.

Table III-1. Ratios of the reflectivity at ν_T or ν_L to that of maximum reflectivity for $NaHF_2$.

	10 degrees		37 degrees	
	Experimental/Theoretical		Experimental/Theoretical	
ν_{2T} (1206 cm^{-1})	0.75	0.72	0.77	.75
ν_{2L} (1244 cm^{-1})	0.70	0.55	0.72	0.89

The corresponding transverse and longitudinal frequencies of transverse and bending vibration of $NaDF_2$ were calculated from the $NaHF_2$ frequencies using both the G matrix ratio and the ratio of the uncoupled bending frequencies. The values of the transverse and the longitudinal frequencies are given below for both methods with the G-matrix calculated frequencies in parenthesis (Table III-2). The G-matrix ratio is 0.7164 compared to the uncoupled absorption frequencies ratio of 0.7202 ($\frac{893}{1240}$). The ratio of the uncoupled ν_2's is probably more accurate, since the G-matrix elements are for a harmonic oscillator.

Table III-2. Bending frequencies for $NaH(D)F_2$.

Vibrational Mode	$NaHF_2$	$NaDF_2$
ν_2 (uncoupled)	1240 cm^{-1}	893 cm^{-1}
ν_{2T}	1206 cm^{-1}	871 (864) cm^{-1}
ν_{2L}	1244 cm^{-1}	898 (891) cm^{-1}

Reflection spectra at 37 degrees as well as 10 degrees, were obtained of single crystalline KHF_2. A single crystal was used for the experiments involving the X-Y scattering plane; while two single crystals were black-waxed together in order to obtain a larger surface for the X-Z scattering face experiments of KHF_2. This should not affect the reflectivity measurements since there is only one crack down the middle of the X-Z face. The black-wax was on the back side of the reflecting face. There are two bending vibrations and they belong to the A_{2u} and E_u symmetry species. The X-Y face for KHF_2 can be easily polished; however, the X-Z faces for the black-waxed crystal are more difficult since the crystal shears very easily. Both faces were observed with an optical microscope and the X-Y face is slightly better than the X-Z face.

All of the reflection spectra reported here were obtained by using the PE-180 with a resolution of 2 cm^{-1} or less. Resolution is more important for KHF_2 than $NaHF_2$ since the quasi-longitudinal mode is sharper than the normal reflection band and that both reflection bands occur in the same reflection arrangement. The 100 percent reflectivity line was set as previously described.

There were six different reflection spectra obtained on KHF_2. These are listed below in Table III-3 along with the expected reflectivities, where Q-A_{2u} represents the quasi-longitudinal mode of the A_{2u} mode. The spectra for each of these experiments are shown in

Figures III-5 to III-10. Also included in the drawings are the theoretical curves for each experiment. Values of 1440 cm^{-1} and 1570 cm^{-1} were used for the transverse and longitudinal frequencies for the ν_3 vibrations. The value of 1440 cm^{-1} is the frequency that Wilkinson reported from his reflection studies (13). The damping constant was estimated at 15 cm^{-1} for the ν_3 vibration compared to Wilkinson's value of 40 cm^{-1}. Changing the damping constant of ν_3 has very little effect on the band shape or position of the ν_2 bands. The ν_L and especially the ν_T frequencies of the ν_3 band has a much larger effect on the ν_2 reflection spectra than does the damping constant.

Table III-3. Types of reflection experiments performed on KHF_2.

Number	θ_i (degrees)	Scattering Face	Plane of Incidence	R Type	Expected Activity
1	10	XY	XZ	R_E	E_u
2	37	XY	XZ	R_E	E_u
3	37	XY	XZ	R_M	E_u & Q-A_{2u}
4	10	XZ	XY	R_E	A_{2u}
5	37	XZ	XY	R_E	A_{2u}
6	37	XZ	YZ	R_M	A_{2u} & Q-E_u

The six reflection spectra cannot be discussed independently when comparing the longitudinal and the transverse frequencies of both the theoretical and experimental curves. The reason is that in one

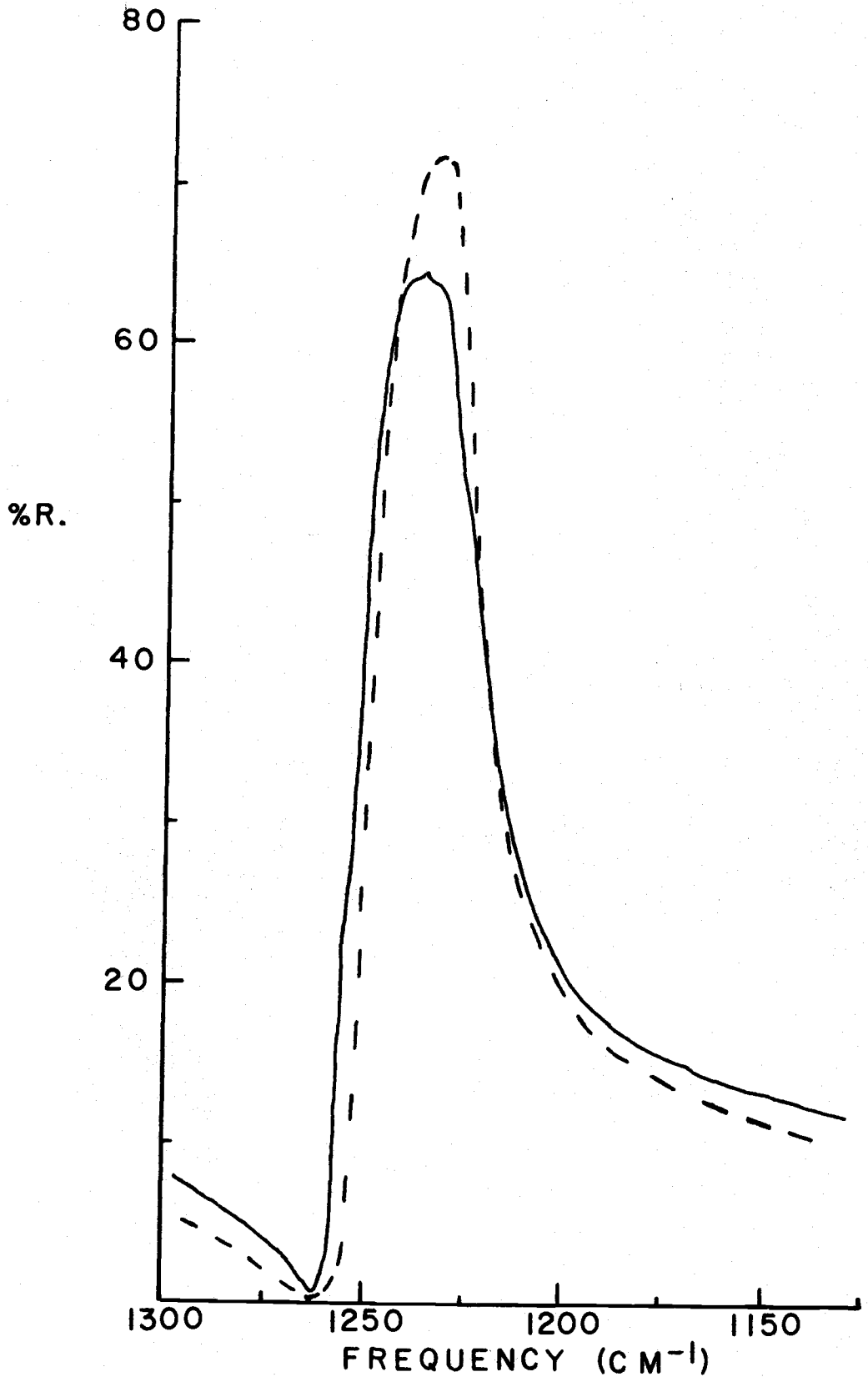
80
60
40
20
%R.
1300
1250
1200
1150
FREQUENCY (C M⁻¹)

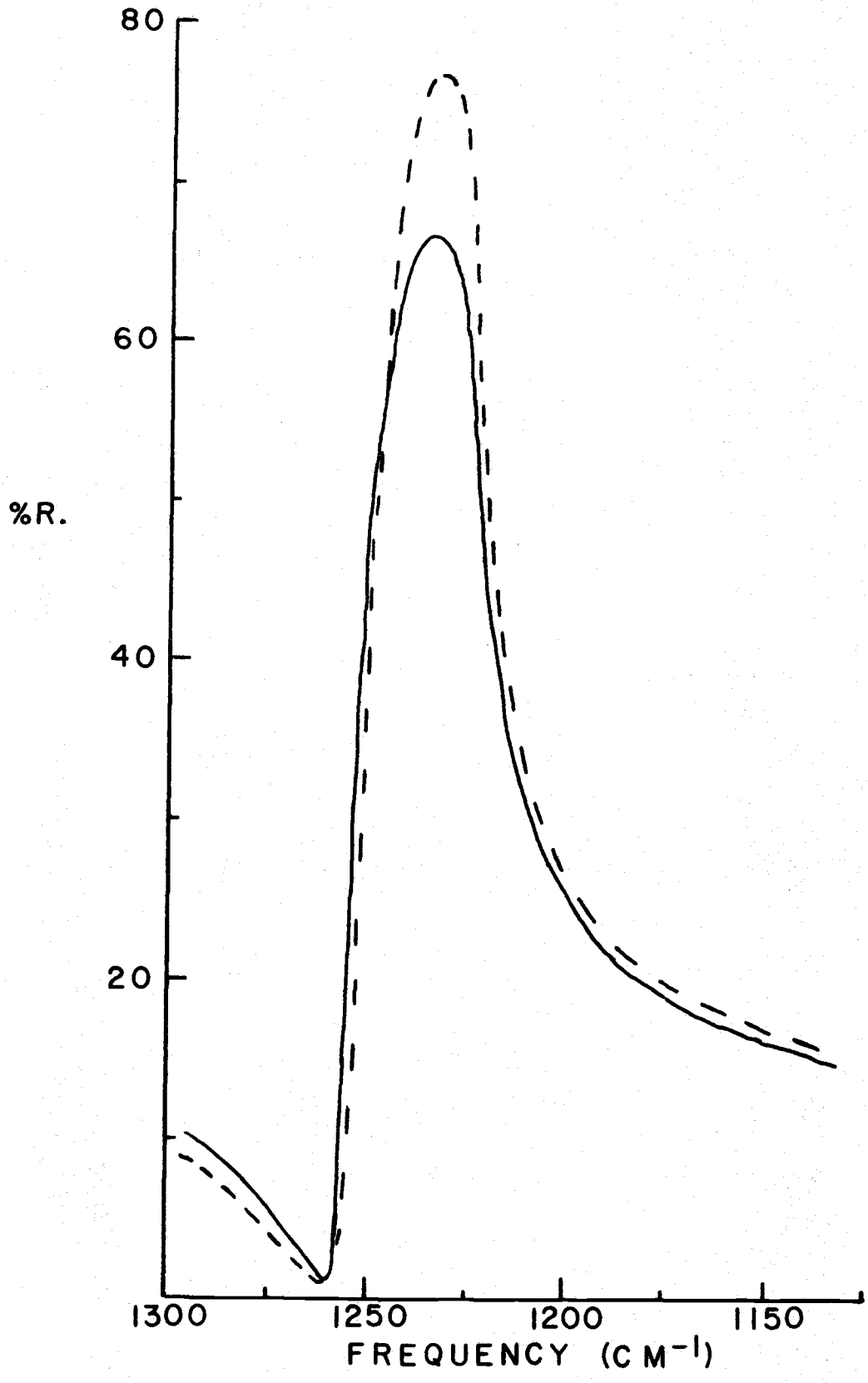
80
60
40
20
%R.
1300
1250
1200
1150
FREQUENCY (C M⁻¹)

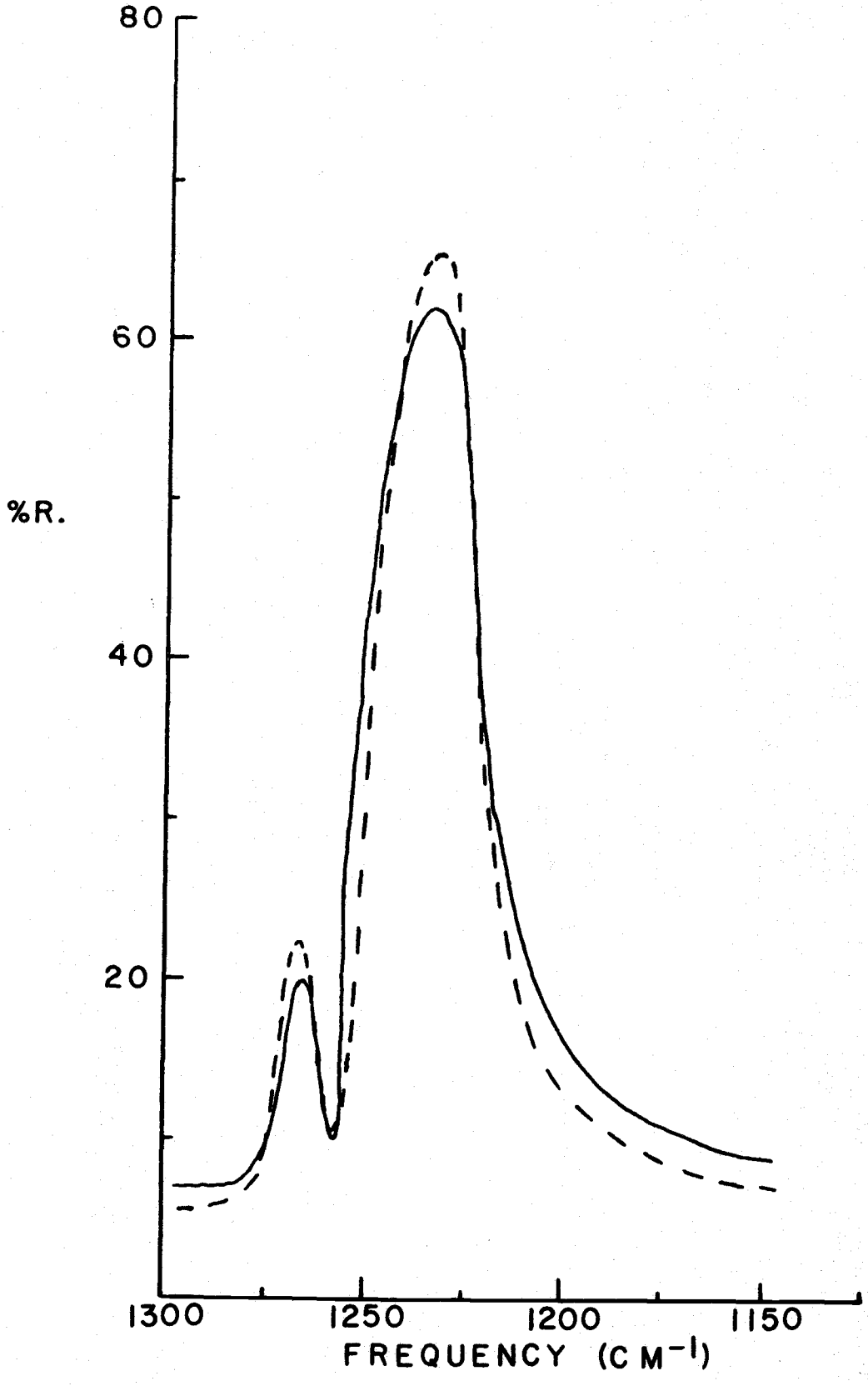
80
60
40
20
%R.
1300
1250
1200
1150
FREQUENCY (C M⁻¹)

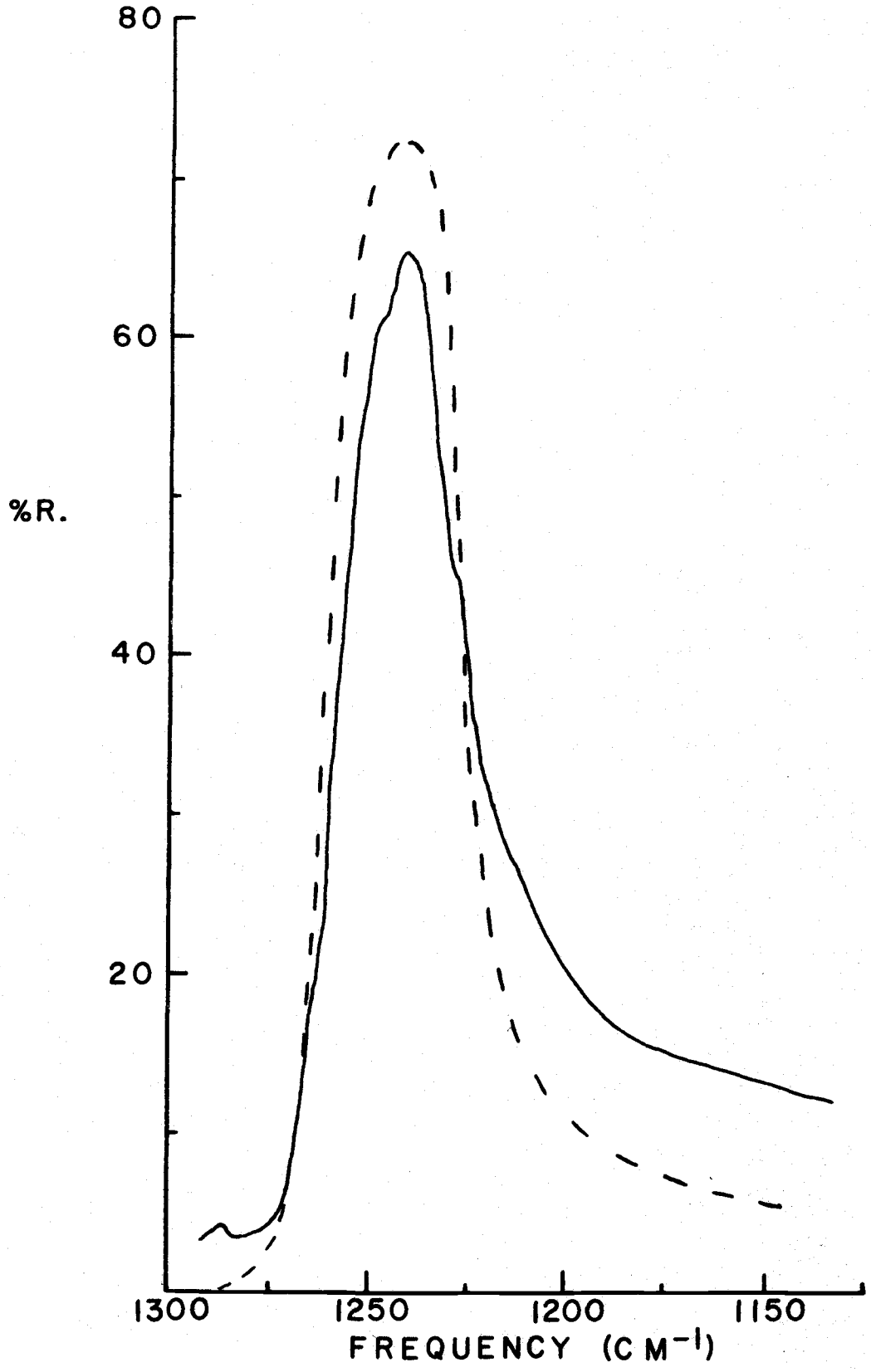
80
60
40
20
%R.
1300
1250
1200
1150
FREQUENCY (C M⁻¹)

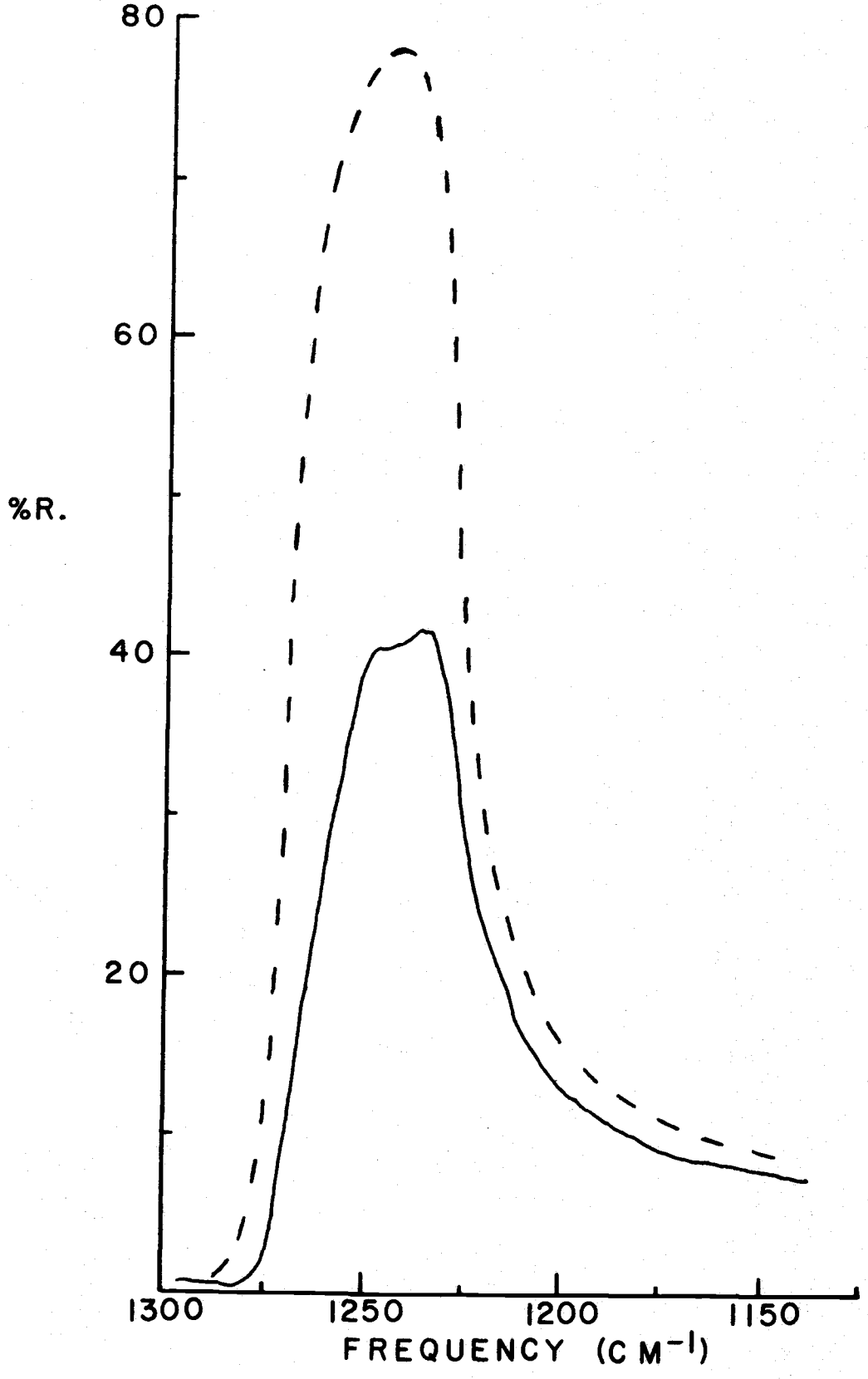
80
60
40
20
%R.
1300
1250
1200
1150
FREQUENCY (C M⁻¹)

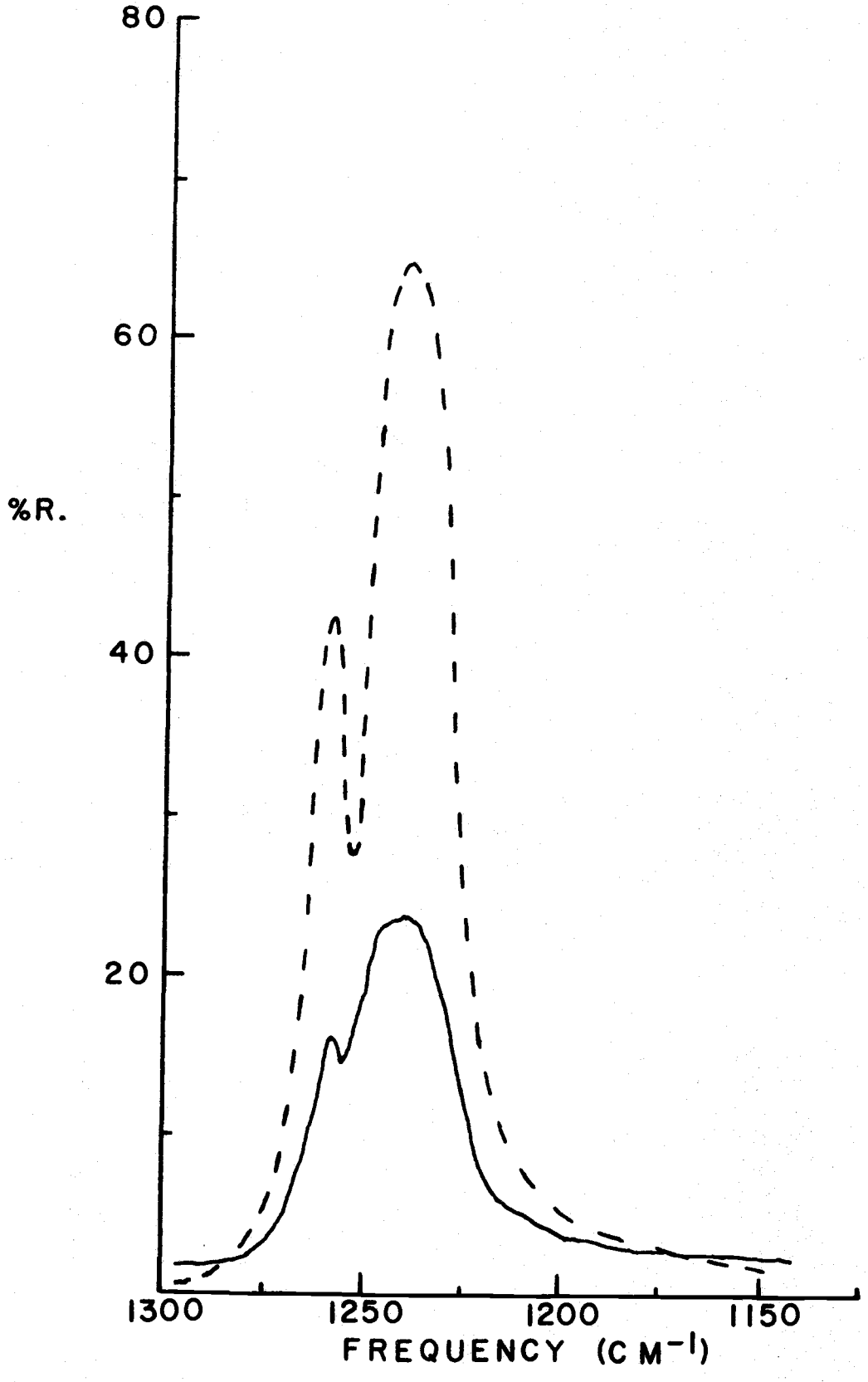
80
60
40
20
%R.
1300
1250
1200
1150
FREQUENCY (C M⁻¹)

experimental arrangement the longitudinal frequency should be increased; while in another arrangement, the longitudinal frequency should be decreased when comparing the theoretical curves to the experimental curves. The transverse and the longitudinal frequencies of the $\nu_2(A_{2u})$ vibration were found to be 1229±3 cm^{-1} and 1262±3 cm^{-1}, respectively; while the corresponding values of the $\nu_2(E_u)$ vibration are 1225±3 cm^{-1} and 1270±7 cm^{-1} (Table III-4). Also, listed in Table III-4 are the frequencies of the ν_3 vibration which were used for the theoretical curves. The damping constants of the two vibrations, $\nu_2(A_{2u})$ and $\nu_2(E_u)$, were varied from 0 to 27 cm^{-1} and were both fixed at 6 cm^{-1}. Approximately ten reflectance spectra were calculated for the A_{2u} mode in which ν_T was varied from 1227 cm^{-1} to 1234 cm^{-1} and ν_L was varied from 1258 to 1265 cm^{-1}; while the ν_T and ν_L for the $\nu_2(E_{2u})$ mode were varied from 1221 cm^{-1} to 1229 cm^{-1} and from 1251 cm^{-1} to 1275 cm^{-1}, respectively. The quasi-longitudinal reflection band was very helpful in estimating Γ for the $\nu_2(A_{2u})$ mode, because the height of the band compared to that of the $\nu_2(E_u)$ band in the same experiment depends on Γ, in much the same way as does a normal (R_E) reflection band. The quasi-longitudinal reflection band for the $\nu_2(E_u)$ mode was not as helpful in determining Γ, since the band overlaps significantly with the $\nu_2(A_{2u})$ band in the same spectrum. The error in the Γ's are estimated to be 2 cm^{-1} and 3 cm^{-1} for the $\nu_2(A_{2u})$, $\nu_2(E_u)$, respectively.

Table III-4. Transverse and longitudinal frequencies associated with the internal modes of KHF_2.

	Assignment	Previous Assignment
$\nu_{2T}(A_{2u})$	1229 cm^{-1}	1234 cm^{-1} [a]
$\nu_{2L}(A_{2u})$	1262 cm^{-1}	
$\nu_{2T}(E_u)$	1225 cm^{-1}	1227 cm^{-1} [a]
$\nu_{2L}(E_u)$	1270 cm^{-1}	
$\nu_{3T}(E_u)$	1440 cm^{-1} [a]	1440 cm^{-1} [a]
$\nu_{3L}(E_u)$	1570 cm^{-1}	

[a]Reference 13.

Since single crystals of KHF_2 can be obtained (Chapter I), the parameters (ν_{2T} and ν_{2L} of both modes) were adjusted such that the theoretical and experimental curves agree in shape as well as position. Initial values of ν_T and ν_L were estimated for both modes in the same way as with the sodium salt. Then these estimated values were the input of the computer program and then the theoretical curves were plotted from the output. The initial values of $\nu_T(A_{2u})$ and $\nu_T(E_u)$ were within 3 cm^{-1} of the final values. The longitudinal frequency for the $\nu_2(A_{2u})$ mode was within 2 cm^{-1} from the estimated frequency. The $\nu_{2L}(A_{2u})$ frequency was aided by the quasi-longitudinal experiment where the longitudinal frequency occurs at approximately one-half of the peak height of the band on the low frequency side. However, the longitudinal frequency $\nu_{2L}(E_u)$ was not aided by its quasi-longitudinal band as much as that of the $\nu_{2L}(A_{2u})$,

since the $\nu_3(E_u)$ vibration is of the same symmetry as that of $\nu_2(E_u)$. In fact, because of this mixing and repeling of the $\nu_2(E_u)$ and $\nu_3(E_u)$ modes, the estimated longitudinal frequency of $\nu_2(E_u)$ was 15 cm^{-1} lower than the final frequency of $\nu_{2L}(E_u)$.

The first figure (III-1) is a R_E experiment with the near normal arrangement. The reflection face is the X-Y plane of the crystal. This arrangement should only allow reflectivity of the $\nu_2(E_u)$ vibrational band. The longitudinal frequency of the theoretical curve could be increased for better agreement, but as mentioned previously it would alter the other theoretical curves. The longitudinal limit would have to be about 1280 cm^{-1} for the best fit for the longitudinal side, and if this was done, the damping constant would have to be changed which would change the slope of the curve. So just a simple increase in the longitudinal limit would not necessarily result in better agreement. Not only does increasing the longitudinal limit affect the longitudinal side of the reflection band, but it changes the transverse side of the band. The $\nu_3(E_u)$ has a large affect on this reflection spectrum since both of the bands are of the same symmetry. This is illustrated by the dip in the reflectivity at about 1260 cm^{-1} in Figures III-5 and III-6 and accounts for the fact that the longitudinal frequency, ν_{2L} is outside the reflection of the band. Thus the two E_u species repel one another in the experiment. Normally, when two bands repel each other, there is also an energy, or in this case reflectivity,

borrowing. However, this will be assumed to be small, since the start of the reflectivity of the ν_3 vibrational band begins immediately after the ν_2 reflection.

The next drawing (Figure III-6) is an R_E experiment using the beam condenser reflection apparatus. The face of the crystal is X-Y. This experiment should only allow the $\nu_2(E_u)$ species as well as $\nu_3(E_u)$. The agreement of the two curves is about the same as that of the near normal arrangement. However, the transverse limit on the theoretical curves should be lowered and the longitudinal frequency increased by approximately one-half that for the prior experiment (Figure III-5).

The last reflection spectrum which has the same face (X-Y) of the crystal is the R_M experiment with an incidence angle of 37 degrees (Figure III-7). This experiment should yield a normal type of reflection for the $\nu_2(E_u)$, but should have a quasi-longitudinal reflection maximum for the $\nu_2(A_{2u})$ mode. The frequency corresponding to maximum reflectivity of this Q-$\nu_2(A_{2u})$ is 1266 cm^{-1} experimentally, while the theoretical peak appears at 1267 cm^{-1}. The Q-$\nu_2 A_{2u}$ frequency of maximum reflectivity (1266 cm^{-1}) was very valuable to confirm the choice of $\nu_{2L}(A_{2u})$ and to reduce the uncertainty in the $\nu_{2L}(A_{2u})$ frequency. The longitudinal frequency of the $\nu_2(A_{2u})$ mode is 1262 cm^{-1}. The general fit of all three experiments on the X-Y face of the crystal is good considering the problems of comparing a

theoretical crystal at θ_i to a real crystal at $\theta_i + \Delta\theta_i$.

The next three figures must be weighed less in determining the longitudinal and transverse frequencies, since the X-Z faces (Black-waxed crystal) do not polish as well as theX-Y face of a single crystal. The first spectrum is the R_E experiment with an angle of incidence of 10 degrees. The optic axis is perpendicular to the plane of incidence. In this arrangement only the $\nu_2(A_{2u})$ should be strictly allowed. The theoretical curve of this spectrum is broader than the experimental curve on the longitudinal side which indicates that the longitudinal limit should be lowered slightly (Figure III-8). However, if this were done, the quasi-longitudinal reflection would also be lowered by at least 6 cm^{-1} and might not appear in the theoretical curve caused by band overlap of the $\nu_2(E_u)$ and $Q\text{-}\nu_2(A_{2u})$.

An R_E experiment of 37 degrees (shown in Figure III-9) is the last reflection spectrum taken of the X-Z face with the optic axis perpendicular to the plane of incidence. It is difficult to compare the reflection bands for this experiment because of the difference in reflectivity between the two curves. The center of the band and the relative position of the longitudinal and transverse frequencies, indicate that the longitudinal limit should be lowered by 5 cm^{-1} and the transverse limit raised by 2 or 3 cm^{-1}. This is indicated below by Table III-5 of the relative heights of the two frequencies compared to the maximum reflectivity of the band. Also, in this spectrum, one

can lower the damping constant to obtain a better fit. This is the case for about one-half of the experiments; while in the other half of the experiments it should be increased.

Table III-5. Ratios of reflectivity at ν_T or ν_L to that of maximum reflectivity for KHF_2.

	Experimental	Theoretical
$\nu_{2T}(A_{2u})$	0.91	0.79
$\nu_{2L}(A_{2u})$	0.59	0.84

The last arrangement is the R_M experiment with an angle of 37 degrees, where the optic axis is parallel to the plane of incidence and the face is the X-Z plane of the crystal. This spectrum should allow the $\nu_2(A_{2u})$ and the Q-$\nu_2(E_u)$ which it does as shown in Figure III-10. However, the quasi-reflection occurs between ν_L and ν_T of the $\nu_2(E_u)$ limits. This can be explained by the presence of the ν_3 band which repels both the regular as well as the quasi-reflection band, as in this spectrum. The agreement between the theoretical and experimental curves could be improved if a higher Γ and/or a higher value of the longitudinal frequency of the $\nu_2(A_{2u})$ were used in the theoretical curve, which contradicts the previous spectrum of a lower Γ and a lower $\nu_{2L}(A_{2u})$.

It should be emphasized that the frequencies of the longitudinal and transverse phonons associated with the bending vibrations were

obtained from a visual least squares method taking all the different reflection experiments into account. This is well illustrated by the last two figures (Figures III-9 and III-10) where the first reflection spectrum (Figure III-9) indicates that the frequency of $\nu_{2L}(A_{2u})$ should be increased; while the second (Figure III-10) spectrum indicates the frequency should be decreased. Estimated errors on the reported longitudinal frequencies of the $\nu_2(A_{2u})$ and $\nu_2(E_u)$ are 3 cm^{-1} and 7 cm^{-1}, respectively; while the corresponding estimated errors of the transverse frequencies are 3 cm^{-1} for both modes.

Finally, the reflection curves clearly show the influence of the $\nu_3(E_u)$ vibrational band upon the $\nu_2(E_u)$ mode; while the $\nu_3(E_u)$ band has very little effect on the $\nu_2(A_{2u})$. This was illustrated by the positions of the longitudinal frequencies of both the $\nu_2(E_u)$ and $\nu_2(A_{2u})$ mode. Therefore, one must be careful in assigning the transverse and/or longitudinal frequencies if there is another band of the same symmetry within a few hundred cm^{-1}.

The transverse and longitudinal frequencies of both bending vibrations of the potassium deuterated bifluoride were calculated from the average ratio of the corresponding uncoupled frequencies (Table III-6).

Table III-6. Bending frequencies of $KH(D)F_2$.

	KHF_2	KDF_2	Ratio
$\nu_2(B_{3u})$ (uncoupled E_u)	1238 cm^{-1}	894 cm^{-1}	0.7221
$\nu_2(B_{1u})$ (uncoupled A_{2u})	1263 cm^{-1}	911 cm^{-1}	0.7213
$\nu_{2T}(A_{2u})$	1229±3 cm^{-1}	887±2 cm^{-1}	
$\nu_{2L}(A_{2u})$	1262±3 cm^{-1}	911±2 cm^{-1}	
$\nu_{2T}(E_u)$	1225±3 cm^{-1}	884±2 cm^{-1}	
$\nu_{2L}(E_u)$	1270±7 cm^{-1}	917±2 cm^{-1}	

IV. OBSERVATION

Observation of the Raman Effect

The preparation of single crystals of KHF_2 was described previously (Chapter II). The larger crystals were cleaved with a razor blade and the edges were sanded with wet-and-dry carborundum paper and polished with jeweler's rouge. The optic axis was checked with an optical microscope and found to be perpendicular to the large face of the crystal. This technique of determining the optic axis of any uniaxial crystal is described in Bunn (25). After cleaving, it was found that the resulting squared base rectangular piped (shown below) can be cleaved at 45 degrees to the one cleaved. This means the KHF_2

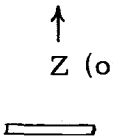

crystal axes would be either X, Y, and Z or $\frac{X+Y}{\sqrt{2}}$, $\frac{X-Y}{\sqrt{2}}$, and Z, depending on the cleavage, where X, Y, and Z are the crystallographic axes. Therefore, the X and Y axes had to be checked.

The axes were checked with a Syntex P_2-Autodiffractometer with a molybdenum target in the department.[2] It was found that the crystal would have to be rotated (approximately 50 degrees) in order to correspond with the true crystallographic axes. Therefore, instead of

[2] I am indebted to Dr. Ted Hopkins for his help in determining the crystal orientation.

sanding and polishing the crystal to line up with the true axes, the crystal was sanded and polished such that the true axes remained just 45 degrees from the crystal cleaved axes (shown below).

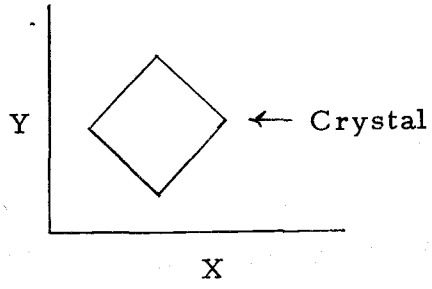

Appearing down the optic (Z) axis

The alignment of the crystal is critical, because the polarizability tensors containing X and Y would mix; however, if the new axes of the crystal were $\frac{X+Y}{\sqrt{2}}$, $\frac{X-Y}{\sqrt{2}}$, and Z the polarized Raman effect would yield data similar to that of a true-axes crystal. This will be discussed in more detail in conjunction with our data.

The crystal was mounted to a goniometer head by black waxing the crystal to a glass rod (3 mm in diameter). It was then slipped into the head and tightened by a set screw. The goniometer allows rotation and translation of the crystal easily with reference to the base. The goniometer in turn was screwed into a mount which can rotate the goniometer freely. The mount that was used, was taken from an optical microscope. This in turn was strapped down to the sample compartment of the instrument with large rubber bands.

Since a large crystal of $NaHF_2$ could not be obtained, Raman

spectra of powdered samples were taken. Crystalline $NaHF_2$ was ground into a fine powder and packed into a capillary tube (1 mm in diameter) with a tungsten rod. Then the tube was placed in capillary holder for the Cary 82 and put into the sample compartment. This technique is quite simple, but polarization data should not be expected.

The Cary 82 Raman spectrophotometer coupled with the 52B Ar^+ laser made by Coherent Radiation was used for all of the Raman spectra. The laser has two high output power lasing lines, 5145 Å and 4880 Å, of which only the 5145 Å was used. The Cary 82 has several important features which will be briefly discussed. First, the triple monochromators allow one to study frequencies close to that of the lasing line and, also obtain a resolution (spectral band width) of less than one cm^{-1} for most samples. Second, a built in scrambler can be inserted to correct for instrumental polarizations. Finally, the laser electric field vector may be easily rotated 90 degrees with a quarter wave plate and the scattered radiation may be studied with an analyzer consisting of a polaroid film; therefore, in laboratory axes with the laser beam striking the sample in the x direction and scattered radiation in the z direction, there would be four different polarizability tensors that can be studied. These would be X(YX)Z, X(YY)Z, X(ZX)Z and Y(ZY)Z arrangements, so the crystal once aligned, does not have to be changed for studying these four polarizability tensors. In addition to this, masking the collecting lens

was found necessary in order to minimize convergent errors. This would enable better polarization studies of a single crystal; however, in decreasing the size of the collecting lens from three inches to ~5/16 of an inch, the signal was reduced. The instrument was calibrated with a 1/3 watt neon lamp, and the frequencies reported are corrected to this calibration.

Anomalous polarization effects appear in the spectra due to the beam convergence of divergence. Porto was the first to recognize that for birefringent crystals (uniaxial crystals) the leakage of other scattering modes that are not strictly allowed can be decreased significantly by reducing the solid angle of both the incident radiation (focus of laser) and the collecting lens (26). This was accomplished by removing the focusing lens of the laser beam and masking the collection lens. The collecting lens was reduced in size from three inches in diameter to approximately 5/16 of an inch in diameter. Since the signal is reduced significantly by both of these precautions, the slit in the Cary 82 had to be widened; hence, resolution was poorer.

The Raman spectrum of $NaHF_2$ will be discussed first. The spectrum is easily interpreted, because there are only two active modes and they are separated by several hundred cm^{-1}. These modes are a librational motion, $R_-(E_g)$ and the internal symmetric stretching vibration, $\nu_1(A_{1g})$, and have been assigned previously by RSM at

145 cm^{-1} and 630.5 cm^{-1}, respectively (Table IV-1) (8). These values agree quite well with our results of 144.5 cm^{-1} and 629.5 cm^{-1}. Polarization studies could not be performed because of the scattering from the faces of the powdered poly-crystalline sample.

Table IV-1. Fundamental frequencies of KHF_2 and $NaHF_2$ observed in the Raman effect.

Vibrational Mode	$NaHF_2$ This Work	$NaHF_2$ Previous Work	
$\nu_1(A_{1g})$	629.5 cm^{-1}	630.5 cm^{-1} [a]	
$R_-(E_g)$	144.5 cm^{-1}	145 cm^{-1} [a]	
		KHF_2	
$\nu_1(A_{1g})$	600 cm^{-1}	596 cm^{-1} [a]	595 cm^{-1} [b]
$\nu_1(B_{2g})$	608.5 cm^{-1}	603 cm^{-1} [a]	603 cm^{-1} [b]
$R_-(E_g)$	143 cm^{-1}		
$R_-(B_{1g})$	139.5 cm^{-1}	143.5 cm^{-1} [a]	136 cm^{-1} [b]
$T_+(E_g)$	100.5 cm^{-1}	104 cm^{-1} [a]	100 cm^{-1} [b]

[a] Reference 8.

[b] Reference 9.

Before a discussion of the results of KHF_2, the i (pa) s convention will be explained. This is a convention that describes the directions of the incoming and the scattering radiation as well as the polarization of each with respect to the crystal axes. The initials stand for the direction of incoming radiation (i), polarization of the incoming radiation (p), the polarization of the scattered radiation

(a-analyzer), and the direction of the scattered radiation being analyzed (s). Since these are referenced with the crystal axes, careful alignment of the crystal with the instrument (laboratory) axes is necessary. To illustrate this convention, an experiment of X(YX)Y type means the laser beam is coming in parallel to the X axis and has its electric field vector parallel to the Y axis. The polaroid is aligned such that it allows only radiation to come through it which is polarized in the X direction, and this radiation is analyzed parallel to the Y axis of the crystal. Notice that the activity is governed by the XY or YX polarizability tensors which are in the parentheses.

If the conditions of no beam convergence and right angle scattering are not satisfied, or if the crystal is twinned, lines may appear in the Raman spectrum which are not allowd by the perfect single crystal selection rules.

The Raman spectra of KHF_2 are more complex than those of the corresponding sodium salt due to the crystal symmetry and a lower site symmetry of the former. The five fundamental modes are $R_-(E_g)$, $R_-(B_{1g})$, $T_+(E_g)$, $\nu_1(B_{2g})$ and $\nu_1(A_{1g})$. This was derived previously (Chapter I) for a crystal that is oriented with X, Y, and Z axes as the laboratory axes. However, since the axes of our crystal were rotated by 45 degrees about the Z axis, this would change some of the polarizability tensors or mix the symmetry-allowed species. If a unitary transformation corresponding to this 45 degree rotation is

performed on each of the polarizability tensors, the resulting polarizability tensor would be the tensor associated with the vibrational mode in the crystal. Upon carrying out this operation upon the polarizability derivative tensor, one finds the new symmetry species for each mode to be $R_-(E_g)$, $R_-(B_{2g})$, $T_+(E_g)$, $\nu_1(B_{1g})$ and $\nu_1(A_{1g})$ (16). Notice that there are only two changes in symmetry of the vibrational modes, namely $R_-(B_{2g})$ and $\nu_1(B_{1g})$. Therefore, these two species have interchanged as far as the activity of the modes. This is illustrated below, where α' is the new polarizability tensor and α, the old. The initial polarizability tensor of a B_{1g} mode can be written;

$$\alpha(B_{1g}) = \begin{pmatrix} a & 0 & 0 \\ 0 & -a & 0 \\ 0 & 0 & 0 \end{pmatrix}$$

now perform the 45 degree rotation upon this α. This is described by

$$\alpha' = R\alpha R^{-1}$$

where

$$R = \frac{1}{2}\begin{pmatrix} \sqrt{2} & \sqrt{2} & 0 \\ -\sqrt{2} & \sqrt{2} & 0 \\ 0 & 0 & 2 \end{pmatrix}$$

is the matrix representation of the rotation and R^{-1} is simply the inverse of R. Solving for the new polarizability tensor one obtains

$$\alpha' = \begin{pmatrix} 0 & a & 0 \\ a & 0 & 0 \\ 0 & 0 & 0 \end{pmatrix} = \alpha(B_{2g})$$

which would correspond to the B_{2g} polarizability tensor. This can easily be done for the $\alpha(B_{2g})$ as well, and it would transform into $\alpha(B_{1g})$.

There are other ways of showing the exchange of the B_{1g} and the B_{2g} symmetry species for our crystal. One is use the other two fold axis as the main axis in correlating from D_{2h} to D_{4h} on a correlation diagram. This also can be pictured by a D orbital scheme in which the $d_{x^2-y^2}$ orbital rotated 45 degrees would be the d_{xy} orbital. This can be done because the d-orbital transform like their corresponding polarizability tensors. However, all three of these methods yield the same result--that is, a perfect exchange occurs between the B_{1g} and the B_{2g} species, and the other symmetry species (E_g and A_{1g}) remain the same for our Raman scattering experiments.

Mathieu and Mathieu were the first to observe the Raman scattering of KHF_2 and reported bands at 603 cm^{-1}, 595 cm^{-1}, 136 cm^{-1} and 100 cm^{-1} (9). Later RSM reported values of 603 cm^{-1}, 596 cm^{-1}, 143.5 cm^{-1} and 104 cm^{-1} (8); however, both of them reported only four of the five fundamental frequencies. RSM suggested that the $R_-(B_{1g}$ and $R_-(E_g)$ modes both occur at 143.5 cm^{-1} from their Raman

scattering experiments of polycrystalline KHF_2. Table IV-1 contains the previous results of KHF_2 as well as the results of this study.

The Raman spectra are shown in Figure IV-1 for the four different polarizability tensors. In order to perform a complete polarization study of KHF_2 all four of these polarizations (ZZ, ZY, XY, and XX) or their equivalent (ZY = ZX) are necessary. The top three spectra were obtained without rotating the crystal (as shown by the same incoming (i) and scattered radiation (s) in the i(pa)s system). All four of the spectra were recorded with a spectral band width of 3 cm^{-1}. Only the top three can be used for comparing the polarizability tensor magnitude because of the different scattering face used in obtaining the fourth spectrum. The inserts in the figures show the number of counts equal to full scale (intensity = 1.0).

The first spectrum, Y(ZY)X orientation, should only allow the E_g modes; thus one should only observe the two fundamentals. Two strong bands were observed, one at 101 cm^{-1} and the other at 143 cm^{-1}; and they are assigned to the $T_+(E_g)$ and $R_-(E_g)$, respectively. Also, a small band appeared at 601 cm^{-1} and was attributed to the leakage of the $\nu_1(A_{1g})$ internal mode. It should be emphasized that masking was critical for the 143 cm^{-1} ($R_-(E_g)$) mode. The assignment of these two modes was aided by Igbal's work on KN_3 (isomorphic to KHF_2) and RbN_3 (27). He found the librational motions at 151 and 147 cm^{-1} and the translational motion at 104 cm^{-1}. This

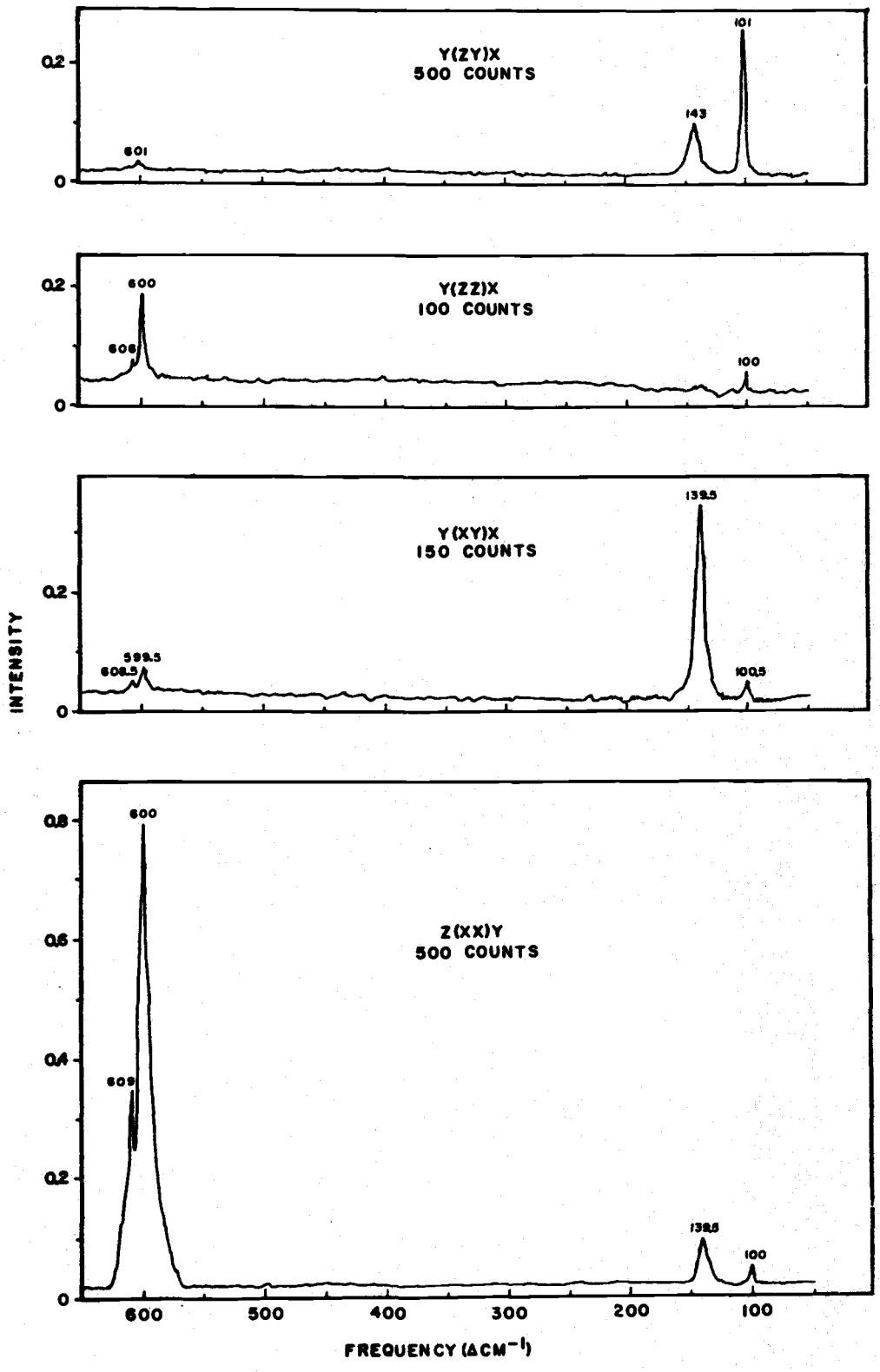
Y(ZY)X
500 COUNTS
101
143
601
0.2
0
Y(ZZ)X
100 COUNTS
600
608
100
0.2
0
Y(XY)X
150 COUNTS
139.5
599.5
608.5
100.5
0.2
0
INTENSITY
Z(XX)Y
500 COUNTS
600
609
138.5
100
0.8
0.6
0.4
0.2
0
600
500
400
300
200
100
FREQUENCY (ΔCM⁻¹)

translational motion $T_+(E_g)$ was assigned at 104 cm^{-1} because of Igbal's reduced mass studies with both the RbN_3 and KN_3. This 104 cm^{-1} (potassium ion) translation should be approximately the same as the (potassium ion) translation of 100.5 cm^{-1} in KHF_2.

The second spectrum in Figure IV-1 shows the Y(ZZ)X configuration, which should allow only the $\nu_1(A_{1g})$ vibration. The 600 cm^{-1} band, by far the strongest peak, is assigned to the $\nu_1(A_{1g})$, while the two weak features at 100 cm^{-1} and 608 cm^{-1} are explained by the leakage of the $T_+(E_g)$ and $\nu_1(B_{2g})$ vibrational modes, respectively.

The crystal cut or cleavage of the KHF_2 crystals is critical for the last two polarization studies. The KHF_2 crystal cleaves very easily in both the (100) and (010) planes, as well as the 45 degree planes of (110) and $(1\bar{1}0)$ planes. The crystal on which the Raman scattering was performed was cleaved along the (110) and $(1\bar{1}0)$ planes.

For both of the last two polarizations, the crystallographic axes were used. Thus, we will label the $\nu_1(B_{2g})$, remembering that the polarizability tensor associated with the $\nu_1(B_{2g})$ mode is really (X Y); while our polarization studies would label it as the (XX) type.

The next spectrum is the Y(XY)X configuration; however, this should allow only the (X^2-Y^2) polarizability tensor because of the cut of the crystal. Therefore, only the B_{1g} mode should be allowed; and,

as is shown in the spectrum, the 139.5 cm^{-1} band is by far the strongest peak which is assigned to the $R_-(B_{1g})$ librational mode. The other weak features appear at 608.5 cm^{-1}, 599.5 cm^{-1} and 100.5 cm^{-1}, which are assigned to the leakage of the $\nu_1(B_{2g})$, $\nu_1(A_{1g})$ and $T_+(Eg)$, respectively.

The last spectrum on Figure IV-1 shows the Z(XX)Y orientation with the XX or YY polarizability tensors allowed. This should allow the totally symmetric vibration A_{1g} as well as the XY polarizability derivative because of the cut of the crystal. The two ν_1 components at 609 cm^{-1} and 600 cm^{-1} are assigned to the B_{2g} and the A_{1g} species, respectively; while the two lower frequency bands at 139.5 cm^{-1} and 100 cm^{-1} are attributed to the leakage of the $R_-(B_{2g})$ and $T_+(E_g)$, respectively.

If one assumes that the N_3^- is an isotope of HF_2^-, one can calculate the librational frequencies of HF_2^- in KHF_2 from those of N_3^- in KN_3. In carrying out this calculation, the predicted librational frequencies for HF_2^- are 127 cm^{-1} and 130 cm^{-1} for the $R_-(B_{1g})$ and $R_-(E_g)$, respectively using Igbal's reported frequencies of 147 cm^{-1} ($R_-(B_{1g})$) and 151 cm^{-1} ($R_-(E_g)$) for KN_3 and bond lengths of 1.13 (H-F) and 1.15 (N-N) (27, 28). Although the space groups (D_{4h}^{18}) are the same for KHF_2 and KN_3, the crystal parameters are larger for KN_3. Therefore one can understand why the calculated frequencies

($127\ cm^{-1}$ and $130\ cm^{-1}$) are lower than the observed frequencies of $139.5\ cm^{-1}$ and $143\ cm^{-1}$ since the force constants would be smaller for a crystal structure which is larger.

V. DIPOLAR COUPLING

Mandel and Mazur have shown that the interaction energy between polar, polarizable molecules can be written

$$V' = V_d + V_{ir} + V_R \quad (29). \tag{V-1}$$

The first term (V_d) contributes to shift in frequency for vibrational modes; while V_{ir} and V_R are related to the infrared and Raman intensities, respectively. These latter two terms shall be ignored since this work is associated with frequency shifts and not with intensities. The dipolar coupling potential can be written (15)

$$V_d = \sum_{ij} -\frac{1}{2} \vec{\mu}'_i \underset{\approx}{T} (\underset{\approx}{E} - \underset{\approx}{\alpha} \underset{\approx}{T})^{-1} \vec{\mu}_j , \tag{V-2}$$

where $\vec{\mu}'$ and $\vec{\mu}$ are $3N$ dimensional row and column vectors, respectively, $\underset{\approx}{T}$, $\underset{\approx}{E}$, and $\underset{\approx}{\alpha}$ are $3N \times 3N$ matrices for a system of N molecules. The $\vec{\mu}'$s are the intrinsic electric dipole moments; $\underset{\approx}{T}$ is the field propagation matrix, $\underset{\approx}{E}$ is the unit matrix, and $\underset{\approx}{\alpha}$ is the polarizability. This above equation represents the potential interaction from one ion at site i to another ion at site j. However, when considering $k = 0$ (all unit cells in phase) vibrational modes, the dimensions of the above expression $(3N)$ are reduced to those of a primitive unit cell by summing the field propagation tensors associated with all equivalent sites. In doing this, one arrives at the

expression for the interaction potential,

$$V_d = -\frac{1}{2}\vec{\mu}' \underset{\approx}{S}\, \underset{\approx}{B}\, \vec{\mu}, \qquad \text{(V-3)}$$

where $\underset{\approx}{S} = \sum_j \underset{\approx}{T}_{ij}$ and $B = (\underset{\approx}{E} - \alpha \underset{\approx}{S})^{-1}$. The field propagation tensor can be written

$$T_{ij} = \frac{3}{r_{ij}^5}(r_j - r_i)(r_j - r_i) - \frac{E}{3 r_{ij}}, \qquad \text{(V-4)}$$

where r_{ij} is the distance between the ion at j and that at i, and $(r_j - r_i)^2$ is a dyadic product.

The field propagation tensor lattice sums $(\underset{\approx}{S})$ were obtained directly using a procedure developed by deWette and Schacher in which the summation is performed in the reciprocal lattice over the Fourier transform of Equation (V-4) (30). The computer program for this procedure has been written by Dickman and the results for $NaHF_2$ and KHF_2 are listed in Tables V-1 and V-2.[3] Some small differences between the S elements in the present calculations and those reported by Frech and Decius are noted in Table V-1 (31). Also listed in Table V-1 are the transverse sums of Frech and Decius (31). The $\underset{\approx}{S}$ sums may differ in direction and there are two different values of $\underset{\approx}{S}$, one for the transverse and the other for the longitudinal wave (15). The $\underset{\approx}{S}$ matrix has the form shown below for the sodium salt

[3] I am indebted to Dr. R.E. Carlson for providing a copy of this program.

Table V-1. The S sums for $NaHF_2$.

$$\underset{\approx}{S} = \begin{pmatrix} \underset{\approx}{S}^{11} & \underset{\approx}{S}^{12} \\ \underset{\approx}{S}^{21} & \underset{\approx}{S}^{22} \end{pmatrix} \qquad \underset{\approx}{S}^{ij} = \begin{pmatrix} S^{ij}_{xx} & S^{ij}_{xy} & S^{ij}_{xz} \\ S^{ij}_{yx} & S^{ij}_{yy} & S^{ij}_{zz} \\ S^{ij}_{zx} & S^{ij}_{zy} & S^{ij}_{zz} \end{pmatrix}$$

$$S^{ij}_{xx} = S^{ij}_{yy}$$

$$S^{ij}_{k\ell} = 0 \quad \text{for} \quad k \neq l$$

$$S^{11} = S^{22}$$

$$S^{21} = S^{12}$$

Sum	Transverse ($\mathring{A}^{-3}$)	Longitudinal ($\mathring{A}^{-3}$)
S^{11}_{xx}	0.13162, 0.13228[a]	-0.13146
S^{12}_{xx}	0.02864, 0.02911[a]	-0.23444
S^{11}_{zz}	-0.00016, -0.00148[a]	-0.26324
S^{12}_{zz}	0.20581, -0.20486[a]	0.05727

[a] Values obtained from Reference 31.

Table V-2. The S sums for KHF_2.

$$S = \begin{pmatrix} S^{11} & S^{12} & S^{13} & S^{14} \\ S^{21} & S^{22} & S^{23} & S^{24} \\ S^{31} & S^{32} & S^{33} & S^{34} \\ S^{41} & S^{42} & S^{43} & S^{44} \end{pmatrix} \qquad \underset{\approx}{S}^{ij} = \begin{pmatrix} S^{ij}_{xx} & S^{ij}_{xy} & S^{ij}_{xz} \\ S^{ij}_{yx} & S^{ij}_{yy} & S^{ij}_{yz} \\ S^{ij}_{zx} & S^{ij}_{zy} & S^{ij}_{zz} \end{pmatrix}$$

$S^{11} = S^{ii}$

$S^{12} = S^{34}$

$S^{13} = S^{14} = S^{23} = S^{24}$

$S^{ij} = S^{ji}$

$S^{ij}_{xx} = S^{ij}_{yy}$

$S^{ij}_{k\ell} = 0 \quad \text{for} \quad \ell \neq k$

Sum	Transverse ($\mathring{A}^{-3}$)	Longitudinal ($\mathring{A}^{-3}$)
S^{11}_{xx}	0.03818	-0.07662
S^{12}_{xx}	0.01804	-0.09676
S^{13}_{xx}	0.04609	-0.06871
S^{11}_{zz}	0.03845	-0.07635
S^{12}_{zz}	0.07874	-0.03606
S^{13}_{zz}	0.02264	-0.09216

$$\underset{\approx}{S}_j = \begin{pmatrix} \underset{\approx}{S}_j^{11} & \underset{\approx}{S}_j^{12} \\ \underset{\approx}{S}_j^{21} & \underset{\approx}{S}_j^{22} \end{pmatrix} \qquad \text{(V-5)}$$

where 1 represents the Na^+ ion and 2 the bifluoride ion (15). The subscript (j) either stands for the transverse (T) or the longitudinal (L) sum. Each element in $\underset{\approx}{S}_j$ can be written in cartesian coordinates as illustrated below.

$$\underset{\approx}{S}_j^{kl} = \begin{pmatrix} S_{xx_j}^{kl} & S_{xy_j}^{kl} & S_{xz_j}^{kl} \\ S_{yx_j}^{kl} & S_{yy_j}^{kl} & S_{yz_j}^{kl} \\ S_{zx_j}^{kl} & S_{zy_j}^{kl} & S_{zz_j}^{kl} \end{pmatrix} \qquad \text{(V-6)}$$

The $\underset{\approx}{S}$ tensor for the potassium salt has a similar form to that for the sodium salt except that $\underset{\approx}{S}_j$ is a four by four matrix instead of a two by two, since there are two K^+ ions (1 and 2 in Table V-2) and two HF_2^- ions (3 and 4 in Table V-2) per primitive cell.

Before the $\underset{\approx}{B}$ tensor can be calculated from the $\underset{\approx}{S}$ sums, one needs to determine the polarizability of the cation, as well as the perpendicular and parallel components of the bifluoride ion polarizability. Frech and Decius have calculated the polarizabilities of the anion assuming a polarizability of the cation finding $\alpha_{11} = 2.27$ and $\alpha_{\perp} = 1.52$ in $NaHF_2$ (31). This calculation requires knowing the

refractive indices along the crystal axes and the $\underset{\approx}{S}$ sums for the transverse waves. This is illustrated below, where n_k is the refractive index; V is the volume of the unit cell and the $\underset{\approx}{a}$ and $\underset{\approx}{B}$ tensors as previously defined. This Equation (V-7) will be applied

$$n_k^2 - 1 = \frac{4\pi}{V} \sum_{ij} (\underset{\approx}{B}_k \underset{\approx}{a}_k)_{ij} \qquad (V-7)$$

for the n_z case of the potassium salt.

The a_z for the primitive unit cell can be written

$$a_z = \begin{pmatrix} a_1 & 0 & 0 & 0 \\ 0 & a_1 & 0 & 0 \\ 0 & 0 & a_\perp & 0 \\ 0 & 0 & 0 & a_\perp \end{pmatrix}, \qquad (V-8)$$

where a_1 and $a_\perp$ represent the polarizability of the potassium ion and the perpendicular polarizability of the anion, respectively. The $a_\perp$ only enters into the z direction (a_z); however for the x and y direction both, a_{11} as well as $a_\perp$ enter into the polarizability tensor ($\underset{\approx}{a}_{x,y}$). A value of 1.03 $\mathring{A}$ (3) was used for a_1 in the calculation of a_{11} and $a_\perp$ (32). Now, since the $\underset{\approx}{B}_k$ and $\underset{\approx}{a}_k$ only contain one unknown, $a_\perp$, (V-7) can be solved readily for $a_\perp$. So, not only does one use the $\underset{\approx}{B}$ sums for calculating the dipole-dipole interaction, but the polarizabilities of the anion. One can now apply

this calculated value of $a_{\perp}$ to the xy direction to determine a_{11}; however, the polarizability tensor for the x and y direction is more complex. The $\underset{\approx}{a}_{xy}$ cannot be separated into two identical direction of x and y, but it can be if one changes to a coordinate system of $(x+y)\frac{1}{\sqrt{2}}$ and $(x-y)\frac{1}{\sqrt{2}}$. The $\underset{\approx}{a}_{xy}$ has the form

$$\underset{\approx}{a}_{xy} = \begin{pmatrix} a_1 & 0 & 0 & 0 \\ 0 & a_1 & 0 & 0 \\ 0 & 0 & a_2 & 0 \\ 0 & 0 & 0 & a_2^1 \end{pmatrix} \tag{V-9}$$

where

$$\underset{\approx}{a}_1 = \begin{pmatrix} a_1 & 0 \\ 0 & a_1 \end{pmatrix}, \tag{V-10}$$

$$a_2 = \frac{1}{2}\begin{pmatrix} a_{11}+a_{\perp} & a_{11}-a_{\perp} \\ a_{11}-a_{\perp} & a_{11}+a_{\perp} \end{pmatrix} \tag{V-11}$$

and

$$a_2^1 = \frac{1}{2}\begin{pmatrix} a_{11}+a_{\perp} & a_{\perp}-a_{11} \\ a_{\perp}-a_{11} & a_{11}+a_{\perp} \end{pmatrix} \tag{V-12}$$

in the x, y and z axes system.

The polarizability tensors a_2 and a_2^1 differ because of the orientation of the two bifluoride ions are different in the unit cell. This can be calculated by the formula

$$a^{i}_{\alpha\beta} = a_{\perp}\delta_{\alpha\beta} + (a_{11}-a_{\perp})\ell^{i}_{\alpha}\ell^{i}_{\beta} , \qquad \text{(V-13)}$$

where ℓ^{i}_{α} and ℓ^{i}_{β} are the direction cosines of the ith ion from the α and β axes respectively.

In the $(x\pm y)/\sqrt{2}$ axis system, a_2 and a^{1}_{2} have the following forms:

$$a_2 = \begin{pmatrix} a_{11} & 0 \\ 0 & a_{\perp} \end{pmatrix} \qquad a^{1}_{2} = \begin{pmatrix} a_{\perp} & 0 \\ 0 & a_{11} \end{pmatrix} \qquad \text{(V-14)}$$

However, in using this coordinate system for calculating a_{11} one also has to transform the $\underset{\approx}{S}$ sums to this system. This can easily be done, since the $\underset{\approx}{S}$ sums for KHF_2 are diagonal. This same procedure was applied to the sodium salt.

A value of 1.03 $\mathring{A}^3$ was used for the polarizability of the potassium ions (a_1) and refractive indexes of 1.331 and 1.354 for n_z and n_x respectively were used in the calculation of $a_{\perp}$ and a_{11} (32,33). Using these values $a_{\perp}$ was found to be 1.60 $\mathring{A}^3$ and a_{11} was 2.03 $\mathring{A}^3$ for the bifluoride ion in KHF_2. Since this same method was previously applied to $NaHF_2$ by Frech and Decius the calculation of $a_{\perp}$ and a_{11} for the sodium salt was not necessary (31). The a's as well as optical properties of both salts are listed in Table V-3.

Table V-3. The polarizabilities and optical constants of $NaHF_2$ and KHF_2.

	$NaHF_2$	KHF_2
n_z	1.328[a]	1.331[a]
n_x	1.261[a]	1.354[a]
$\alpha_{\parallel}$	0.292[b]	1.03 $\AA^3$
$\alpha_{\perp}$	1.52[c]	1.60 $\AA^3$
α_{II}	2.27[c]	2.03 $\AA^3$

[a]Reference 33.

[b]Reference 32.

[c]Reference 31.

The $\underset{\approx}{B}$ matrices are tabulated in Tables V-4 and V-5. Thus the dipole-dipole interaction potential can be calculated. However, instead of calculating this potential one calculates the force constant for this potential. From the force constant calculation one can compare the theoretical shift in frequency to the experimental observed value.

The force constant for either the sodium or the potassium bifluoride bending vibration can be expressed in terms of an uncoupled force constant F_0 and the force constant associated with the dipolar coupling potential (shown below). The F_d was obtained by taking the

$$F = F_0 + F_d \tag{V-15}$$

second derivative of the potential V_d with respect to the molecular

Table V-4. The B matrix elements for $NaHF_2$.

$$B = \begin{pmatrix} \underset{\approx}{B}^{11} & \underset{\approx}{B}^{12} \\ \underset{\approx}{B}^{21} & \underset{\approx}{B}^{22} \end{pmatrix} \qquad \underset{\approx}{B}^{ij} = \begin{pmatrix} B^{ij}_{xx} & B^{ij}_{xy} & B^{ij}_{xz} \\ B^{ij}_{yx} & B^{ij}_{yy} & B^{ij}_{yz} \\ B^{ij}_{zx} & B^{ij}_{zy} & B^{ij}_{zz} \end{pmatrix}$$

$$B^{ij}_{xx} = B^{ij}_{yy}$$

$$B^{ij}_{k\ell} = 0 \quad \text{for} \quad k \neq l$$

Sum	Transverse	Longitudinal
B^{11}_{xx}	1.04062	0.73337
B^{12}_{xx}	0.01087	-0.04185
B^{21}_{xx}	0.05662	-0.21782
B^{22}_{xx}	1.25064	0.84590
B^{11}_{zz}	1.02882	0.92985
B^{12}_{zz}	0.06181	-0.00973
B^{21}_{zz}	0.48049	-0.07567
B^{22}_{zz}	1.02850	0.62679

Table V-5. The B matrix elements for KHF_2.

$$\underset{\approx}{B} = \begin{pmatrix} B^{11} & B^{12} & B^{13} & B^{14} \\ B^{21} & B^{22} & B^{23} & B^{24} \\ B^{31} & B^{32} & B^{33} & B^{34} \\ B^{41} & B^{42} & B^{43} & B^{44} \end{pmatrix} \qquad \underset{\approx}{B}^{ij} = \begin{pmatrix} B^{ij}_{\alpha\alpha} & B^{ij}_{\alpha\beta} & B^{ij}_{\alpha z} \\ B^{ij}_{\beta\alpha} & B^{ij}_{\beta\beta} & B^{ij}_{\beta z} \\ B^{ij}_{z\alpha} & B^{ij}_{z\beta} & B^{ij}_{zz} \end{pmatrix}$$

$$\alpha = \frac{1}{\sqrt{2}}(x+y) \qquad \beta = \frac{1}{\sqrt{2}}(x-y) \qquad \underset{\approx}{B}^{ij}_{k\ell} = 0,\ k \neq 1 \qquad \underset{\approx}{B}_{\alpha\alpha} = \underset{\approx}{B}_{\beta\beta}$$

B Sum	Transverse	Longitudinal
$B^{11}_{zz} = B^{22}_{zz}$	1.05141	0.94810
$B^{12}_{zz} = B^{21}_{zz}$	0.09126	-0.01206
$B^{13}_{zz} = B^{14}_{zz} = B^{23}_{zz} = B^{24}_{zz}$	0.03279	-0.07530
$B^{31}_{zz} = B^{32}_{zz} = B^{41}_{zz} = B^{42}_{zz}$	0.05094	-0.11699
$B^{33}_{zz} = B^{44}_{zz}$	1.09988	0.91232
$B^{34}_{zz} = B^{43}_{zz}$	0.14859	-0.02712
$B^{11}_{\alpha\alpha} = B^{22}_{\alpha\alpha}$	1.05150	0.94473
$B^{12}_{\alpha\alpha} = B^{21}_{\alpha\alpha}$	0.03031	-0.07645
$B^{13}_{\alpha\alpha} = B^{23}_{\alpha\alpha}$	0.05745	-0.04694
$B^{14}_{\alpha\alpha} = B^{24}_{\alpha\alpha}$	0.05694	-0.04652
$B^{31}_{\alpha\alpha} = B^{32}_{\alpha\alpha}$	0.11341	-0.09266
$B^{33}_{\alpha\alpha}$	1.09752	0.89602
$B^{34}_{\alpha\alpha}$	0.05434	-0.14534
$B^{41}_{\alpha\alpha} = B^{42}_{\alpha\alpha}$	0.08833	-0.07217
$B^{43}_{\alpha\alpha}$	0.04271	-0.11425
$B^{44}_{\alpha\alpha}$	1.07557	0.92004

coordinate system. This can be written

$$F_d = -\hat{\mu}' \underset{\approx}{S} \underset{\approx}{B} \hat{\mu}\left(\frac{\partial \mu}{\partial q}\right)_0^2 , \qquad \text{(V-16)}$$

where the $\hat{\mu}'$ and $\hat{\mu}$ are defined as unit row and column vectors representing the direction of the vibrational mode in the same coordinate system that $\underset{\approx}{S}$ and $\underset{\approx}{B}$ are expressed (Table V-6 contains a listing of $\hat{\mu}'$ and $\hat{\mu}$). Substituting Equation (V-2) into Equation (V-1) and converting from force constants to frequencies associated with these force constant one obtains the relation

$$\nu_j^2 = \nu_0^2 - K\mu' \underset{\approx}{S}_j \underset{\approx}{B}_j \mu\left(\frac{\partial \mu}{\partial q}\right)_0^2 , \qquad \text{(V-17)}$$

where $K = \dfrac{10^{24}\ \text{cm}^{-3}}{4\pi^2 c^2} = 28.190\ \text{sec}^2\text{cm}^{-5}$ and ν_0 is the uncoupled frequency. This derivation follows directly from $|FG - \lambda E| = 0$ and has been presented elsewhere (15, 34). The subscript j denotes that this equation can be solved for the transverse frequency ν_T as well as the longitudinal frequency ν_L with the corresponding lattice sums (shown below). Subtracting Equation (V-18) from Equation (V-19) one

$$\nu_T^2 = \nu_0^2 - K\hat{\mu}' S_T \underset{\approx}{B}_T \hat{\mu}\left(\frac{\partial \mu}{\partial q}\right)_0^2 \qquad \text{(V-18)}$$

$$\nu_L^2 = \nu_0^2 - K\hat{\mu}' \underset{\approx}{S}_L \underset{\approx}{B}_L \hat{\mu}\left(\frac{\partial \mu}{\partial q}\right)_0^2 \qquad \text{(V-19)}$$

arrives at the relation

$$\nu_L^2 - \nu_T^2 = K\hat{\mu}'(\underset{\approx}{S}_T \underset{\approx}{B}_T - \underset{\approx}{S}_L \underset{\approx}{B}_L)\hat{\mu}(\frac{\partial\mu}{\partial q})_0^2 , \qquad \text{(V-20)}$$

which can readily be solved for $(\frac{\partial\mu}{\partial q})_0^2$. Then substituting the value of $(\frac{\partial\mu}{\partial q})_0$ into either Equation (V-18) or Equation (V-19), a value of ν_0 can be obtained. The values of ν_0 and $(\frac{\partial\mu}{\partial q})_0$ for the bending vibration of $NaH(D)F_2$ and $KH(D)F_2$ are listed in Tables V-7 and V-8, respectively.

Table V-6. Unit dipole moment derivative vectors for $NaHF_2$ and KHF_2.

	μ' (where $\mu_{ij} = \mu'_{ji}$)
$\underline{NaHF_2}$	
$\nu_2(E_u)$	(000100) or (000010)
$\underline{KHF_2}$	
$\nu_2(A_{2u})$	$(1/\sqrt{2})$(000000001001)
$\nu_2(B_{1u})$	$(1/\sqrt{2})$(00000000100-1)
$\nu_2(E_u)$	(1/2)(0000001101-10) or (1/2)(000000110-110) in x, y, z
$\nu_2(E_u)$	$(1/\sqrt{2})$(000000100010) or $(1/\sqrt{2})$(0000001000-10) in α, β, z

Table V-7. Frequencies and dipole moment derivatives of the bending vibrations of $NaHF_2$ and $NaDF_2$ with the error indicated in parenthesis.

	$NaHF_2$	$NaDF_2$
$\nu_{2T}(E_u)$	1206(3) cm^{-1}	869(2) cm^{-1}
$\nu_{2L}(E_u)$	1244(3) cm^{-1}	896(2) cm^{-1}
$(\frac{\partial \mu}{\partial q})_0$	$\pm 111(4)\, cm^{3/2} sec^{-1}$	$\pm 80(3)\, cm^{3/2} sec^{-1}$
ν_0 (calculated)	1229(4) cm^{-1}	885(3) cm^{-1}
ν_0 (observed)	1240 cm^{-1}	893 cm^{-1}

Experimental values of the uncoupled frequencies are also listed in Tables V-7 and V-8. In both cases, the dilute KDF_2 and the dilute KHF_2, the $\nu_2(E_u)$ uncoupled frequencies were taken to be the lower frequency bands. The reason is the E_u uncoupled species (B_{3u}) should be more intense and should be lower in frequency since there would be a greater probability of interacting with the other isotopic species surrounding it. The distance between the center of the bifluoride (hydrogen atom) ion to the adjacent bifluoride ion in the plane is 4.02 Å while the nearest bifluoride in the z direction is 6.81 Å.

The ν_2 (uncoupled) frequencies are higher than the ν_2's (calculated) for both of the $\nu_2(E_u)$ vibrations of $NaH(D)F_2$ and for both of the $\nu_2(A_{2u})$ uncoupled vibrations of $KH(D)F_2$; however, the theory

Table V-8. Frequencies and dipole moment derivatives of the bending modes of KHF_2 and KDF_2 with the error indicated in parenthesis.

	KHF_2	KDF_2
A_{2u} Mode		
ν_{2T}	1229(3) cm^{-1}	887(2) cm^{-1}
ν_{2L}	1262(3) cm^{-1}	911(2) cm^{-1}
$(\frac{\partial\mu}{\partial q})_0$	±115(4) $cm^{3/2}sec^{-1}$	±83(3) $cm^{3/2}sec^{-1}$
ν_0 (calculated)	1250(4) cm^{-1}	902(3) cm^{-1}
ν_0 (observed)	1263 cm^{-1}	911 cm^{-1}
E_u Mode		
$\nu_{2T}(E_u)$	1225(3) cm^{-1}	884(2) cm^{-1}
$\nu_{2L}(E_u)$	1270(7) cm^{-1}	917(5) cm^{-1}
$(\frac{\partial\mu}{\partial q})_0(E_u)$	202(14) $cm^{3/2}sec^{-1}$	147(10) $cm^{3/2}sec^{-1}$
ν_0 (calculated	1247(6) cm^{-1}	900(4) cm^{-1}
ν_0 (observed)	1238 cm^{-1}	894 cm^{-1}
B_{1u} Mode		
ν (calculated)	1254(4) cm^{-1}	905(3) cm^{-1}

predicts most of the shift in frequency from the coupled vibrations. The corresponding dipole moment derivatives of these vibrational modes agree quite well, 111 $cm^{3/2}sec^{-1}$ to 115 $cm^{3/2}sec^{-1}$ and 80 $cm^{3/2}sec^{-1}$ to 83 $cm^{3/2}sec^{-1}$ of the deuterated species.

The uncoupled frequencies of the $\nu_2(E_u)$ vibration are lower than the calculated ν_0's for KHF_2. This might be explained by the closeness of the adjacent bifluoride ion in the plane, in particular the fluorine atoms, which could couple the bending vibration through a short range force.

Also included in Table V-8 are the theoretical values for the inactive $\nu_2(B_{1u})$ mode of KHF_2 and KDF_2. These were obtained by using $(\frac{\partial \mu}{\partial q})_0$, $\underset{\approx}{S}$, $\underset{\approx}{B}$ and V_0 from the $\nu_2(A_{2u})$ mode and substituting the $\hat{\mu}'$ and $\hat{\mu}$ of the $\nu_2(B_{1u})$ species (Table V-6) into Equation (V-17). This can be done, since the $\nu_2(B_{1u})$ mode can be represented by an out-of-phase $\nu_2(A_{2u})$ vibration. This is shown below for the two molecules in the unit cell of KHF_2.

A_{2u} 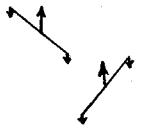 B_{1u} 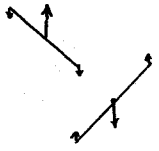

where the arrows indicate the motion of the hydrogen (↑) and the fluorine atoms (↓) in (HF_2^-). Therefore, only a change in sign of the unit dipole moment derivative vectors is necessary. Values of 905 cm^{-1} and 1254 cm^{-1} were calculated for the $\nu_2(B_{1u})$ modes of KDF_2 and KHF_2, respectively.

VI. DISCUSSION

The experimental uncoupled frequencies and the theoretical values of ν_0 do not agree as one would expect; however, the theoretical ν_0's do show the shift to higher frequencies from the coupled vibrational modes. Therefore, the dipole-dipole interaction is not the only interaction potential that is perturbing these frequencies. Both the ν_0's (calculated for the $\nu_2(E_u)$ of $NaHF_2$ and $\nu_2(A_{2u})$ of KHF_2 are lower than the experimental uncoupled (ν_0's) frequencies. This can be explained by the presence of short or long range forces that were turned off as well as the dipole-dipole force. However, the $\nu_2(E_u)$ mode is just the opposite, the frequency observed is less than predicted. This might be explained by the short range force of the hydrogen with the adjacent fluorine atom. The distance between the hydrogen atom and fluorine atom is 2.72 $\mathring{A}$, and considering the electronegativity and a possibility of "long" hydorgen bond between the adjacent fluorine and hydrogen, this type of short range force is likely. This type of force would continue to operate even in the dilute isotopically substituted salts; however, one should expect this force to be slightly higher for hydrogen than deuterium because of the amplitude of vibration is larger.

It was illustrated in Chapter III, that two different angles of incidence could be helpful in assigning the ν_T and ν_L to a vibrational

mode. This is especially true for a quasi-longitudinal experiment which the vibrational mode in question does not have the same symmetry of any of the other vibrational bands in that region. Normally the longitudinal frequency appears on one-half the height of the quasi-longitudinal reflection band at the low frequency side. Also, this quasi-longitudinal spectrum depends in a way similar on $\nu_L^2 - \nu_T^2$ and Γ to a normal reflection band. Since the dielectric constant behavior of the quasi-reflection experiment is different than the normal reflection experiment, this method is more independent from the normal experiment than is the regular R_E experiment with an oblique angle ($\theta_i > 15$ degrees). Therefore, this should be of great use in determining the longitudinal and transverse frequencies of a vibrational mode.

Assigning the ν_T and ν_L frequencies was found to be more difficult if there was another strong vibrational mode of the same symmetry in that region. This explains why the estimated error in $\nu_{2L}(E_u)$ of KHF_2 was larger than the other ν_T and ν_L errors. The reflectivity behavior of the two interacting fundamentals is similar to that of a resonance occurring. This was illustrated by the quasi-longitudinal peak at 1256 cm^{-1} compared to the longitudinal frequency of 1270 cm^{-1}. With this large repulsing of the $\nu_2(E_u)$ and $\nu_3(E_u)$ bands, there is a corresponding mixing of the wave functions.

Thus, this might explain the large $(\frac{\partial \mu}{\partial q})_0$ value (202 $cm^{3/2} sec^{-1}$) compared to the other bending vibrations, $(\frac{\partial \mu}{\partial q})_0$ of 110 $cm^{3/2} sec^{-1}$ and 115 $cm^{3/2} sec^{-1}$. The $(\frac{\partial \mu}{\partial q})_0$ for the ν_3 mode is 383 $cm^{3/2} sec^{-1}$, using values of 1440 for ν_T and 1570 for ν_L. Although this was calculated using the harmonic oscillator approximation, it does give a rough approximation to $(\frac{\partial \mu}{\partial q})_0$. This value of 383 $cm^{3/2} sec^{-1}$ makes the ν_3 mode of (HF_2^-) the strongest infrared band that is presently known. Since there is an interaction between the $\nu_2(E_u)$ and $\nu_3 E_u$, it is quite conceivable that the $(\frac{\partial \mu}{\partial q})_0$ of the $\nu_2(E_u)$ mode could be increased by a factor of two from the mixing with $\nu_3(E_u)$.

There are several other methods of calculating $(\frac{\partial \mu}{\partial q})_0$ for a vibrational mode from the transverse and the longitudinal frequencies. These methods are: 1) Assume that the crystal is cubic (35); 2) Ignore all of the polarizabilities, α's = 0; 3) Ignore the polarizability of the cation, $\alpha_1 = 0$. The results of calculating $(\frac{\partial \mu}{\partial q})_0$ by each of these assumptions as well as our method of calculating $(\frac{\partial \mu}{\partial q})_0$, including all the polarizabilities (all α), are shown below in Table VI-1. It is interesting that ignoring all the polarizabilities is in good agreement with the method of including all of the polarizabilities for the $\nu_2(E_u)$ mode of $NaHF_2$ and the $\nu_2(A_{2u})$ mode of KHF_2; while they are in poor agreement for the $\nu_2(E_u)$ mode of KHF_2. Also, notice that the cubic model is a relatively good model for calculating $(\frac{\partial \mu}{\partial q})_0$

for the ν_2 modes of both crystals.

Table VI-1. Values of $(\partial\mu/\partial q)$ in $cm^{3/2} sec^{-1}$ for the bending vibrations of $NaHF_2$ and KHF_2 by different methods.

Vibrational Mode	Cubic	α's = 0	$\alpha_1 = 0$	all α's
$\nu_2(E_u)$ of $NaHF_2$	±118	±112	±110	±111
$\nu_2(A_{2u})$ of KHF_2	±119	±113	±110	±115
$\nu_2(E_u)$ of KHF_2	±197	±186	±205	±202

The fifth active Raman fundamental was found in this work. The $R_-(B_{1g})$ and $R_-(E_g)$ were separated by their different polarizability tensors. This was made possible by masking the collective lens and not focusing the laser on the single crystal KHF_2 sample. These two bands, 139.5 cm^{-1} and 143 cm^{-1}, could not be separated in the same spectrum, since the half-widths were too large.

Finally, it has been shown that the frequency of maximum absorption does not have to coincide with the transverse frequency associated with the vibrational mode. This is illustrated by the ν_2 modes of $NaHF_2$ and KHF_2, for which the frequency at maximum absorption occurs above and below the transverse frequencies for the bending vibrations of $NaHF_2$ and KHF_2, respectively. Therefore, one should determine the transverse frequency through reflectivity measurements rather than by transmission experiments.

BIBLIOGRAPHY

1. E.F. Westrum Jr. and K.S. Pitzer. Thermodynamics of the System KHF_2-KF-HF, Including Heat Capaciticies and Entropies of KHF_2 and KF. The Nature of the Hydrogen Bond in KHF_2. Journal of the American Chemical Society 71:1940. 1949.

2. E.F. Westrum Jr. and G.A. Burney. Thermodynamics of the Monohydrogen Difluorides. II. Heat Capacities of Lithium and Sodium Monohydrogen Difluorides from 6 to 305°K. The Journal of Physical Chemistry 65:344. 1961.

3. B.L. McGaw and J.A. Ibers. Nature of the Hydrogen Bond in Sodium Acid Fluoride. The Journal of Chemical Physics 39:2677. 1963.

4. J.A. Ibers. Refinement of Peterson and Levy's Neutron Diffraction Data on KHF_2. The Journal of Chemical Physics 40:402. 1964.

5. Frederick Halverson. The Use of Deuterium in the Analysis of Vibrational Spectra. Reviews of Modern Physics 19:87. 1947.

6. A.R. Ubbelohde. Structure and Thermal Properties associated with Some Hydrogen Bonds in Crystals. III Further Examples of the Isotope Effect. Royal Society of London Proceeding A-173: 417. 1939.

7. H. Boutin, G.J. Safford and V. Brajovic. Study of Low-Frequency Molecular Motions in HF, KHF_2, KH_2F_3, and NaH_2F_3 The Journal of Chemical Physics 39:3135. 1963.

8. J.J. Rush, L.W. Schroeder and A.J. Melveger. Dynamics of Sodium and Potassium Bifluoride: Infrared, Raman, and Neutron Studies. The Journal of Chemical Physics 56:2793. 1972.

9. J.P. Mathieu and L. Couture Mathieu. Spectres de Raman de Monocristaux de Fluorure acide de Potassium. Académie des Sciences Comptes Rendus 230:1054. 1950.

10. J.A.A. Ketelaar. The Infrared Absorption and Reflection Spectra of KHF_2 and KDF_2. The Journal of Chemical Physics 9:775. 1941.

11. P.A. Giguere and K. Sathianandan. Lattice Vibrations in KHF_2 and $NaHF_2$. Canadian Journal of Physics 45:2439. 1967.

12. J.A.A. Ketelaar and W. Vedder. The Infrared Spectrum of KHF_2. The Journal of Chemical Physics 19:654. 1951.

13. G.R. Wilkinson. Molecular Dynamics and Structure of Solids. National Bureau of Standards Special Publication 301. 1969. p. 107.

14. D.F. Hornig and G.L. Hiebert. Structure and Molecular Interaction in HX-DX Mixed Crystals. The Journal of Chemical Physics 27:752. 1957.

15. J.C. Decius. Dipolar Coupling and Molecular Vibration in Crystals. I. General Theory. The Journal of Chemical Physics 49:1387. 1968.

16. E. Bright Wilson Jr., J.C. Decius, and Paul C. Cross. Molecular Vibrations. New York, McGraw-Hill, 1955.

17. S. Bhagarantam and T. Venkatarayudu. Theory of Groups and its Applications to Physical Problems. Andhra University Press, 1951.

18. J.A. Salthouse and J.C. Waddington. New Mechanism for the Broadening of Hydrogen Stretching Peak on Hydrogen Bonding. The Journal of Chemical Physics 48:5274. 1968.

19. J.A.A. Ketelaar, C. Haas, and J. van der Elsken. Infrared Absorption Spectra of Bifluorides in Alkali Halide Disks. The Formation of Mixed Crystals. The Journal of Chemical Physics 24:624. 1956.

20. J.A.A. Ketelaar. The Absorption and Reflection Spectra of KHF_2, KDF_2 and $RbHF_2$ in Relation to the Constitution of the Bifluoride Ion. Recueil Des Travaux Chimiques Des Pays-Bas 60:523. 1941.

21. G.L. Cote and H.W. Thompson. Infra-red Spectra and the Solid State. III. Potassium Bifluoride. Proceedings of the Royal Society A 210:206. 1951.

22. K.S. Pitzer and E. F. Westrum. The Nature of the Hydrogen Bond in KHF_2. The Journal of Chemical Physics 15:526. 1947.

23. Max Born and Kun Huang. Dynamical Theory of Crystal Lattices. Oxford, Clavendon Press, 1954.

24. O.S. Heavens. Optical Properties of Thin Solid Films. New York, Dover Publications. 1955. p. 95.

25. C.W. Bunn. Chemical Crystallography. Oxford, Oxford University Press. 1946.

26. S.P.S. Porto, J.A. Giornmaine, and T.C. Damen. Depolarization of Raman Scattering in Calcite. Physical Review 147:608. 1966.

27. Zafar Iqbal. Lattice Mode Raman Effect in KN_3-Type Crystals The Journal of Chemical Physics 53:3763. 1970.

28. Ralph W.G. Wyckoff. Crystal Structures II. New York, Interscience Publishers, 1964. p. 277.

29. M. Mandel and P. Mazur. Molecular Theory of Dielectric Polarization. Physica 24:116. 1958.

30. F.W. deWette and G.E. Schacher. Internal Field in General Dipole Lattices. Physical Review 137:78. 1965.

31. Roger Frech and J.C. Decius. Dipolar Coupling and Molecular Vibrations in Crystals. III. Polarizabilities of Molecular Anions and the Internal Field in Some Rhombohedral Crystals. The Journal of Chemical Physics 51:5315. 1969.

32. Jean Pirenne and Eddy Kartheuser. On the Refractivity of Ionic Crystals. Physica 30:2005. 1964.

33. H. Inslay et al. Optical Properties and X-Ray Diffraction Data for Some Inorganic Fluoride and Chloride Compounds. (U.S. Atomic Energy Commission, ORNL-2192). p. 16.

34. Roger Frech and J.C. Decius. Dipolar Coupling and Molecular Vibrations in Crystals. II. Rhombohedral Lattices. The Journal of Chemical Physics 51:1536. 1969.

35. C. Haas and D. Hornig. Calculation of Dipole Derivatives from Infrared Reflection Spectra or Raman Spectra of Crystals. The Journal of Chemical Physics 26:707. 1957.